# A sunlight responsive metal-organic framework system for sustainable water desalination

*Ranwen Ou,[1,2,8] Huacheng Zhang,[1,8] Vinh X. Truong,[3,4,8] Lian Zhang,[1] Hanaa M. Hegab,[1] Li Han,[5] Jue Hou,[1] Xiwang Zhang,[1] Ana Deletic,[6] Lei Jiang,[1,7] George P. Simon,[4] and Huanting Wang[1,*]*

[1] Department of Chemical Engineering, Monash University, Clayton, VIC 3800, Australia Email: huanting.wang@monash.edu

[2] College of the Environmental & Ecology, Xiamen University, Xiamen, Fujian 361102, PR China

[3] Monash Institute of Medical Engineering, Monash University, Clayton, VIC 3800, Australia

[4] Department of Materials Science and Engineering, Monash University, Clayton, VIC 3800, Australia

[5] School of Chemical Engineering and Energy, Zhengzhou University, Zhengzhou 450001, China

[6] School of Civil and Environmental Engineering, The University of New South Wales, Sydney, NSW 2052, Australia

[7] Key Laboratory of Bioinspired Materials and Interfacial Science, Technical Institute of Physics and Chemistry, Chinese Academy of Sciences, Beijing 100190, People's Republic of China

[8] R. Ou, H. Zhang, and V. X. Truong contributed equally.

## SUPPLEMENTARY NOTES

### Supplementary Note 1 | Methods

*Materials.* Aluminum nitrate nonahydrate ($Al(NO_3)_3 \cdot 9H_2O$), terephthalic acid ($H_2BDC$), and α, α'-azoisobutyronitrile (AIBN) were purchased from Sigma Aldrich. Lithium chloride (LiCl), sodium chloride (NaCl), and sea salts (s9883) were supplied by Sigma Aldrich. The chemicals used for the synthesis of spiropyran acrylate were purchased form Sigma Aldrich, including indoline, tolunene, 2-bromoethanol, diethyl ether, piperidine, benzaldehyde, trienthyl amine, dichloromethane, acryloyl chloride, hydrochloric acid, $NaHCO_3$, brine, and $MgSO_4$. Potassium chloride (KCl), magnesium chloride hexahydrate ($MgCl_2 \cdot 6H_2O$), calcium chloride dihydrate ($CaCl_2 \cdot 2H_2O$), sodium hydroxide (NaOH), and ethanol were purchased from Merck.

*Synthesis and characterization of spiropyran (SP) acrylate.* 1′-(2-acryloxyethyl)-3′, 3′-dimethyl-6-nitrospiro-(2H-1-benzopyran-2, 2′-indoline) is abbreviated as spiropyran acrylate in this study. The synthesis procedures are shown in Supplementary Fig. 1.

To a solution of indoline (5 g, 31 mmol) in tolunene (50 mL) was added 2-bromoethanol (4.7 g, 38 mmol) and the solution was heated at 110 °C with stirring for 10 h. Upon cooling to room temperature the formed pink precipitate was filtered, washed with diethyl ether (100 mL) and used directly in the next step (yield: 8.4 g, 95%).

The above product (2.0 g, 7.0 mmol) was dissolved in ethanol (20 mL) followed by addition of piperidine (0.77 mL, 7.7 mmol) and benzaldehyde (1.78 g, 10.7 mmol) and the reaction mixture was refluxed for 5 h. After cooling to room temperature, the mixture was stirred for an additional hour on an ice bath. The formed precipitate was collected and washed with ice cold ethanol to give product as violet crystal (1.5 g, 4.5 mmol, 64%). $^1H$ NMR: (400 MHz, $d_6$-

DMSO) δ: 7.96 (dd, J = 5.5, 3.3 Hz), 7.83 (dd, J = 5.8, 2.9 Hz, 1H, H4), 7.61–7.53 (m), 4.62–4.56 (t, J = 5.1 Hz, 2H, HA), 3.90–3.84 (t, J = 5.0 Hz, 2H), 2.83 (s), 1.55 (s).

Spiropyran hydroxyl (0.45 g, 1.29 mmol) and trienthyl amine (0.15 g, 1.5 mmol) were dissolved in dry dichloromethane (50 mL) under nitrogen and the solution was cooled on an ice bath. A solution of acryloyl chloride (0.15 g, 0.33 mol) in dichloromethane (100 mL) was added dropwise and the resultant mixture was stirred for 4 hours at ambient temperature. The resultant solution was washed with 0.1 M HCl solution (100 mL), saturated $NaHCO_3$ solution (100 mL), brine (100 mL) and dried over $MgSO_4$. Evaporation of the solution provided product as yellow solid (0.35 g, 71%).

H NMR (270 MHz; $CDCl_3$; TMS): δ (ppm) = 1.16, 1.28 (s, 6H, $–C(CH_3)_2$), 3.38–3.61 (m, 2H, $–NCH_2CH_2–$), 4.31 (t, 2H, $–OCH_2CH_2–$), 5.82 (d, 1H, –CHCHH), 5.86 (d, 1H, –CCHCH–), 6.00–6.10 (m, 1H, $–CHCH_2$), 6.34–6.40 (d, 1H, –CHCHH), 6.69 (d, 1H, –CCHCH–), 6.74 (d, 1H, ArH), 6.87–6.92 (m, 2H, ArH), 7.07–7.10 (m, 1H, ArH), 7.17–7.23 (m, 1H, ArH), 2H, ArH).

*Synthesis of MIL-53.* The MIL-53 was synthesized under hydrothermal condition according to Ref 1. 2.60 g of $Al(NO_3)_3·9H_2O$ and 0.576 g of $H_2BDC$ were added into 10 mL water in a 50 mL Telfon-lined autoclave. The autoclave was sealed and placed in oven at 150 °C for 24 hours. The obtained white powder was centrifuged and washed several times with pure water until the pH of supernatant stable at 4-5. The as-prepared MIL-53 was then dried in 60 °C oven overnight.

*Synthesis of MIL-53-330 °C.* The as-prepared MIL-53 was emptied pore by heat treatment in air before further functionalization. The MIL-53 powder was placed in a ceramic boat in a temperature-programmed box furnace that heated to 330 °C at a heating rate of 5 °C $min^{-1}$,

then stayed at 330 °C for 5 hours. A brown powder was obtained after calcination in air. The calcined MIL-53 (0.020 g) exhibited a weak acidic pH of 5.84 in water (pH 7, 20 mL).

MIL-53 was selected in our study due to its high surface area, suitable pore size, breathing effect, and high water-stability. Firstly, the reported MIL-53 (Al) exhibits a Langmuir surface area of 1590 $m^2$ $g^{-1}$. The MIL-53 (Al) fabricated in our study showed a Brunauer-Emmett-Teller surface area of 875 $m^2$ $g^{-1}$, and a Langmuir surface area of 1077.0 $m^2$ $g^{-1}$, which can provide the composite adsorbent with high porosity for beneficial adsorption and desorption.

Secondly, MIL-53 is well-known for its breathing effect, which exhibits two consecutive breathing transitions upon adsorption of some molecules (e.g., $CO_2$, $H_2O$)[1,2]. The empty MIL-53 framework is expanded with a pore size of 8.5 Å. The pores become contracted (2.6×13.6 Å) while partially filled, and further adsorption can reopen the pores to the expanded state (8.5×8.5 Å)[3]. This highly flexible framework and proper pore size allow the entry of spiropyran (SP) molecules (~5.4×5.8×11.6 Å) into the MOF channels.

Thirdly, MIL-53 with expanded pores and contracted pores show distinct X-ray powder diffraction (XRD) patterns, providing a simple way to determine the framework structure. After calcination of the as-prepared MIL-53 (Al), the XRD pattern shows that the framework is partially filled and in contracted state (Supplementary Fig. 2 in the Supplementary Material). After the introduction of PSP into MIL-53 (Al), it becomes the expanded state, demonstrating the successful fabrication of PSP-MIL-53.

Fourthly, MIL-53 has good water stability. The study of Li *et al.* showed that water stable MOFs could be categorized into three major types, and the first type is metal carboxylate frameworks consisting of high-valence metal ions[4]. MIL-53 (Al) is composed of $Al^{3+}$ and terephthalic acid, which meets the requirement of water stable MOFs. What's more, MIL-53 (Al) has been investigated as adsorbent in aqueous solution, showing good water stability[5,6].

*Synthesis of PSP-MIL-53.* The PSP-MIL-53 was prepared according to Ref [7]. 0.04 g of MIL-53-330 °C, 0.025 g of spiropyran acrylate, and 0.01 g of AIBN were added into 1 mL ethanol. The suspension was stirred for 1-14 days before evaporation of ethanol in fume hood until it was visibly dry. The sample was polymerized in oven at 70 °C for 2 days. The sample was then washed with ethanol and water until the conductivity of supernatant less than 5 μS $cm^{-1}$. The obtained PSP-MIL-53 was dried in 60 °C oven overnight for characterization.

*Characterization.* A Rigaku Miniflex 600 X-ray diffractometer was applied to determine the X-ray diffraction (XRD) patterns at 40 kV and 25 mA at a scanning rate of 10 ° $min^{-1}$ and 2$\theta$ range of 5–60°. The UV-Vis spectra were recorded using a UV-Vis spectrophotometer (UV mini 1240). The conductivity of salt solutions was characterized by a laboratory conductivity meter (Cond 730, inoLab). The thermogravimetric data was measured by a Thermal Gravimetric Infra-Red hyphenated system (TGIR, PerkinElmer) performed at a temperature range of 50 – 800 °C, temperature scanning rate of 40 °C $min^{-1}$, in a 20 mL $min^{-1}$ air flow. Scanning electron microscope images were taken by Nova NanoSEM 450 and Magellan 400 microscope (FEG, SEM, FEI, USA). $N_2$ adsorption-desorption isotherm was collected by a surface characterization analyzer (3 Flex, micromeritics, USA).

*NaCl content of PSP-MIL-53.* The NaCl content of PSP-MI-53 was determined by Scanning Electron Microscopy / Energy Dispersive X-Ray Spectroscopy (SEM-EDS) analysis. In this experiment, PSP-MIL-53 was used to adsorb $Na^+$ and $Cl^-$ in 1,000 ppm NaCl solution under dark condition. After that, the sample was regenerated under visible light irradiation. Then, the original PSP-MIL-53, NaCl adsorbed PSP-MIL-53, and the regenerated PSP-MIL-53 were collected and dried for EDS analysis to determine the relevant NaCl content on the basis of sodium amount. The salt adsorbed PSP-MIL-53 was collected and washed with water to remove NaCl adsorbed on the crystal surface for characterization.

*Wettability of PSP-MIL-53.* The water contact angle of PSP-MIL-53 was determined by a contact angle goniometer (Dataphysis OCA15, Dataphysics, Germany). Firstly, the PSP-MIL-53 powder was pressed into tablets using a press machine (Quick Press KBr Pellet Kit, International Crystal Laboratories). After 30 minutes of exposure to room lighting, the contact angle of the tablet was measured with ~1 μL of water droplet. Secondly, the PSP-MIL-53 tablet was kept in dark for more than 3 hours before the water contact angle measurement. Thirdly, the tablet was exposed to room lighting for 30 minutes before another water contact angle measurement. Fourthly, the tablet was irradiated with UV light for 1 hour, then measured for water contact angle.

*Ion adsorption loading of PSP-MIL-53.* Salt solutions, including LiCl, NaCl, KCl, $MgCl_2$, and $CaCl_2$, were used for the measurement of adsorption loading. 0.05 g of PSP-MIL-53 and 15.00 mL of salt solution (pH 8) were put in a 50 mL centrifuge tube. The pH values of salt solutions were adjusted by 0.01 M NaOH solution. The adsorption occurred under UV (254 nm, p/n 90-0001-05, UVP) or dark. The UV light intensity irradiated on the adsorbent and solution was determined to be ~270 μW $cm^{-2}$ by a radiometer (FZ-A, photoelectric instrument factory of Beijing Normal University, China). After the adsorption of salt, the mixture of PSP-MIL-53-MCl and solution was centrifuged, and the supernatant was collected in another tube for measurement of conductivity. The ion adsorption loading (mmol $g^{-1}$) was calculated as follows:

$$Ion\ adsorption\ loading = \frac{n \cdot C \cdot V}{M_S \cdot w}$$

where $n$ is the number of cations and anions of a salt. $C$ (mg $L^{-1}$) is the concentration difference of the salt solution before and after adsorption determined by the conductivity meter. $V$ (L) is the volume of salt solution, $Ms$ (mol $g^{-1}$) is the molecular weight of the salt, and $w$ (g) is the weight of PSP-MIL-53 sample.

*Desorption of PSP-MIL-53.* Visible light source with three different intensities were used for the regeneration of PSP-MIL-53, including room lighting (0.13 mW $cm^{-2}$), 0.1 sun (~10 mW $cm^{-2}$), and one sun (~100 mW $cm^{-2}$). A sunlight simulator (CHF-XM-500W, TrusTech, China) was used to generate sunlight with intensity of 0.1 sun and one sun. 15.00 mL of water (pH 8) was added to the salt adsorbed PSP-MIL-53 with visible light irradiation. Then, the sample was centrifuged after a certain of time, and washed until the conductivity of supernatant ≤5 μS $cm^{-1}$. The desorbed sample was dried in 60 °C oven for further uses. As for the regeneration of adsorbent in single-column setup, water was added into column with visible light illumination.

*Cycling performance of PSP-MIL-53.* For the cycling experiment of various salts, the adsorption was conducted in dark, and desorption was performed in room lighting of the lab. 10,000 ppm salt solutions were used for the adsorption, while water (pH 8) used for desorption. 10 adsorption and desorption cycles were performed.

*Adsorption performance of PSP-MIL-53 in single-column setup.* The single-column has an inner diameter of 0.6 cm. A certain amount of PSP-MIL-53 was put into the single-column setup with a sample density of 607 g $L^{-1}$. 1,000, 10,000, and 35,000 ppm NaCl solutions were individually added into the column for the breakthrough curves measurement. The water drained at the bottom of the column at 1, 2, 3, 4, 5, 10, 15, 20, 30, 45, 60, 90, 120, 180, 240, and 300 min(s) were collected for analysis. The salt concentration of the collected water was determined by the conductivity meter. The filtration flux was controlled by the valve at the bottom of the column to be ~100 or ~1,000 L $m^{-2}$ $h^{-1}$ (LMH).

*Synthetic brackish water and seawater desalination by PSP-MIL-53.* Synthetic brackish water with 2,233 ppm salts, including 1,083 ppm $Cl^-$, 215 ppm $SO_4^{2-}$. 25 ppm $NO_3^-$, 171 ppm $HCO_3^-$, 448 ppm $Na^+$, 127 ppm $Ca^{2+}$, and 136 ppm $Mg^{2+}$, was prepared according to Ref [8]. The pH of synthetic brackish water was 7.8. 35,000 ppm synthetic seawater was prepared by dissolving

1.75 g of sea salts (s9883, Sigma Aldrich) in pure water to form a 50 g solution. The synthetic seawater showed a pH of 8.3. The salt waters were desalted by passing through the PSP-MIL-53-packed single-column setup.

For brackish water desalination, 0.13 g of PSP-MIL-53 was packed in the column, and 4.50 mL of treated brackish water was collected for analysis. In terms of seawater desalination, 0.63 g of PSP-MIL-53 was packed in the column, and 1.71 g of treated seawater was collected for analysis. The ions concentration of synthetic brackish water ($HCO_3^-$, $SO_4^{2-}$, $Cl^-$, $NO_3^-$, $Ca^{2+}$, $Mg^{2+}$, and $Na^+$) and seawater ($HCO_3^-$, $SO_4^{2-}$, $Cl^-$, $Ca^{2+}$, $Mg^{2+}$, $Na^+$, and $K^+$) and PSP-MIL-53 treated solutions were sent to ALS Environmental (Melbourne, Australia) for analysis. Both original and treated synthetic salt waters were diluted before sending for analysis.

**Supplementary Note 2 | Characterization of PSP-MIL-53**

MIL-53 (Al) was synthesized hydrothermally in water as described in Supplementary Note 1. As shown in Supplementary Fig. 2, the as-prepared MIL-53 was emptied pores by calcination at 330 °C before the accommodation of spiropyran acrylate in ethanol. After the evaporation of solvent (ethanol), the spiropyran acrylate entrapped in MIL-53 was polymerized at 70 °C for 2 days with initiator. The powder obtained was washed with water and ethanol before drying for further use. The as-prepared MIL-53 was a white powder, while the calcined MIL-53-330 °C was a brown powder (Supplementary Fig. 2f). After modifying with polyspiropyran, PSP-MIL-53 was a brown-pink powder. Supplementary Fig. 4 shows the morphology of as-prepared MIL-53, MIL-53-330 °C, and PSP-MIL-53. The as-prepared MIL-53 are irregular particles with smooth surface and edges. After calcination at 330 °C, the particles of MIL-53-330 °C became smaller with rougher surface and shape edges. The size of PSP-MIL-53 became even smaller, while they were connected and covered with polymer.

MIL-53 is well-known for its significant breathing effect upon emptying and filling its channels. When the framework is emptied or fully filled, the channel is extended (Supplementary Figs. 2a and d). The adsorption of water molecules in the empty framework results in the contracted channel (Supplementary Figs. 2b and e). The empty pore MIL-53 fabricated in this study exhibited a BET surface area of 874.5 $m^2 g^{-1}$, and a Langmuir surface area of 1077.0 $m^2 g^{-1}$, with a channel size of 8.5 Å (Supplementary Fig. 3). It has been reported that the hydrous MIL-53 (contracted) shows a channel size of 2.6×13.6 Å. The molecular size of SP and MC are ~11.5 and ~12.5 Å, respectively. Therefore, the flexible framework of MIL-53 could allow the entrance of spiropyran molecules into the pores. On the other hand, due to the larger molecular size of polyspiropyran and the transformation of framework after fully filling, MIL-53 could provide proper confinement of the polymer chains. As shown in Supplementary Fig. 2f, the calcined MIL-53-330 °C exhibited the XRD pattern of contracted MIL-53 (Supplementary Fig. 2e) because of the adsorption of air moisture, while several peaks of the as-prepared MIL-53 were found. After the accommodation of polyspiropyran, the framework of MIL-53 was fully filled, exhibiting the XRD pattern of empty pore MIL-53 (Supplementary Fig. 2d). The vastly changed XRD pattern before and after accommodation of PSP demonstrated the successful introduction of the polymer inside the framework of MIL-53. What's more, the 8.5 Å channel size could reasonably confine the polyspiropyran. The SEM images in Supplementary Fig. 4 showed that MIL-53 particles were covered by a thin layer of PSP.

Both MIL-53-330 °C and PSP-MIL-53 are stable in water (Supplementary Fig. 7). After stirring in water for 30 days, MIL-53-330 °C showed the same XRD pattern as the original one, while the particles became a bit smaller. After 10 adsorption and desorption cycles, the XRD pattern and morphology of PSP-MIL-53 demonstrated its good water-stability (Supplementary Fig. 7). The XRD pattern of PSP-MIL-53 before and after adsorption cycles show very similar

pattern, but not the same. That may be due to the adsorption of water in PSP-MIL-53 and the breathing effect of MIL-53. Firstly, previous studies showed that compare to the XRD pattern of dehydrated MOFs, the hydrated metal organic framework shows broader XRD peak, which might overlap peaks nearby[6,9-12]. On the other hand, some of the peaks might be weaken due to the inclusion of water. Boyd *et al.* developed two metal organic frameworks Al-PMOF and Al-PyrMOF[12]. After immersing the MOFs in water for 7 days, two nearby peaks overlapped and were combined into one peak. Meanwhile, some of the peaks were weaken while some strengthen. However, there is no loss of crystallinity of these MOFs because the characteristic peaks were remained. The study of Vu *et al.* also suggested that the dehydrated MIL-53 (Fe) showed narrow and sharp peaks, while the hydrated one exhibited broad peaks with few peaks combined[6]. After ion adsorption in aqueous solution, PSP-MIL-53 became hydrated. During the drying process, the evaporation of water molecules inside MOFs was blocked by the thin layer of polyspiropyran on surface, resulting in a hydrated PSP-MIL-53.

Secondly, the MIL-53 is well known for its breathing effect, which exhibits two consecutive breathing transitions upon adsorption of some molecules (e.g., $CO_2$, $H_2O$)[1,2]. The empty MIL-53 framework is expanded with a pore size of 8.5 Å. The pores become contracted (2.6×13.6 Å) while partially filled, and further adsorption can reopen the pores to the expanded state (8.5×8.5 Å)[3]. Interestingly, MIL-53 with expanded pores and contracted pores show distinct X-ray powder diffraction (XRD) patterns, providing a simple way to determine the framework structure. The inclusion of water in PSP-MIL-53 may swell the PSP, further opening the framework of MIL-53. In addition, 98% of adsorbed ions and ion adsorption loading were recovered during the regeneration process. Thus, there is about 2% of salts adsorbed by PSP-MIL-53 left in the adsorbent, which may also further expand the framework.

As shown in Supplementary Fig. 7f, the simulated XRD patterns of MIL-53 with contracted and expanded framework are added for comparison. The MIL-53 (ht) with expanded

framework has characteristic peaks at 8.7°, 10.6°, 15.1°, 17.4°, 18.5°, 20.0°, 25.1°, 26.3°, and 32.9°. By contrast, the MIL-53 (lt) with contracted framework has characteristic peaks at 9.3°, 12.5°, 17.8°, 18.3°, 18.8°, 19.6°, 20.8°, 23.4°, 26.3°, 26.9°, 27.3°, 30.5°, 32.5°, and 35.7°. The as-prepared PSP-MIL-53 showed XRD peaks at 8.8°, 9.4°, 10.2°, 10.8°, 15.0°, 16.6°, 17.6°, 18.3°, 20.2°, 21.9°, 25.0°, 26.5°, 30.2°, and 32.8°, showing peaks from both the MIL-53 (lt) and MIL-53 (ht). After 10 cycles, the XRD peaks of PSP-MIL-53 were 8.8°, 10.2°, 10.8°, 15.0°, 16.6°, 17.6°, 18.0°, 20.2°, 21.9°, 25.0°, 26.5°, 30.2°, and 32.8°. It has all the characteristic peaks of MIL-53 (ht), demonstrating the expanded framework of PSP-MIL-53 after adsorption-desorption cycles, and the good stability of PSP-MIL-53. Therefore, the XRD patterns showed no loss of crystallinity upon adsorption cycles.

**Supplementary Note 3 | Polyspiropyran loading amount of PSP-MIL-53**

During the preparation of PSP-MIL-53, the spiropyran acrylate was stirred with MIL-53 in ethanol for 1, 3, 7, or 14 days before polymerization to yield the composite with different polymer loading amount. The PSP loading amount of PSP-MIL-53 was then determined by thermogravimetric analysis in air flow. As shown in Supplementary Fig. 8, the combustion of PSP started at 136 °C in air, and ended at 347 °C. For the TGA curve of MIL-53-330 °C, there was a weight loss before 112 °C due to the loss of water molecules. Then, it started combusting at 581 °C and ended at 710 °C. The distinct combustion patterns of PSP and MIL-53-330 °C would help determining the PSP loading amount of the composites. As shown in Supplementary Fig. 9, when the immersion time before polymerization increased from 1, 3, 7, and 14 days, the PSP loading amount were 15.6, 22.5, 28.7, and 36.3 wt.%, respectively.

The composites with different amount of PSP were then used to adsorb salt in 1,000 ppm NaCl solution under UV 254 nm. The relevant ion adsorption capacities were 0.37, 0.96, 0.57,

and 0.23 mmol $g^{-1}$ with the increasing loading of 15.6, 22.5, 28.7, and 36.3 wt.%, respectively. The PSP-MIL-53 with 22.5 wt.% polymer loading exhibited optimized salt adsorption. That is due to the competition between the amount of adsorption sites and their accessibility. Theoretically, larger amount of PSP would endow the composite with more adsorption sites, resulting in higher ion adsorption loading. However, if the channels of MIL-53 were partially/fully blocked by the polymers, the ions could not reach part of the adsorption sites inside the framework, resulting in lower adsorption. Therefore, PSP-MIL-53 with a PSP loading amount of 22.5 wt.% will be used for further characterization in this study.

**Supplementary Note 4 | pH influence on adsorption and desorption of PSP-MIL-53**

Fig. 2c shows the UV-Vis spectra of spiropyran and merocyanine activated at the pH of 6, 8, and 9. According to the literature, the band located at ~272-296 nm is contributed to the π-π* electronic transition of the indoline part of SP, while the band at ~323-351 nm is attributed to the chromene part. After excitation, MC shows a band at ~550-600 nm in most non-polar solvents, which is due to the formation of the extended π-conjugation between the indolium and chromene moieties (Fig. 2d). In this study, SP solution was colorless in 1,000 ppm NaCl solution, and the spectra of SP (black) showed two peaks at 271 and 349 nm, respectively. The SP was stimulated under dark at different pH to be MC in 1,000 ppm NaCl solution. At the pH of 8, the excited MC solution was pink, and a strong peak at 512 nm was found in its UV-Vis spectra, indicating the formation of extended π-conjugation. However, at the pH of 6, the solution was yellow, and the peak at 512 nm was weak, suggesting that small amount of extended π-conjugation formed. At the pH of 9, the solution became pale orange, while the peak at 512 nm could be barely recognized due to the loss of extended π-conjugation.

The amphoteric and zwitterionic structure of merocyanine is crucial for the adsorption of $Na^+$ and $Cl^-$ simultaneously. As shown in Fig. 2d, the surplus $H^+$ would bind with the phenolate groups, hindering the adsorption of $Na^+$. In contrast, the surplus $OH^-$ might combine with the indolium groups, hindering the adsorption of $Cl^-$. A solution pH of 8 endowed the PSP-MIL-53 with optimized ion adsorption loading.

On the other hand, the environmental pH affects the regeneration performance (Supplementary Fig. 13). At acidic pH (e.g., 6), the adsorbent was partially regenerated (39 %) due to the formation of protonated spiropyran ($SPH^+$, Supplementary Fig. 10a). However, at slightly alkaline pH (e.g., 8), 98 % of ion adsorption capacity could be recovered.

**Supplementary Note 5 | The adsorption and desorption performance of PSP-MIL-53 in a single-column setup**

As described in the Experimental detailed in Supplementary Note 1, 1,000, 10,000, and 35,000 ppm NaCl solutions were filtrated through the single-column setup packed with PSP-MIL-53. The breakthrough curves are shown in Supplementary Fig. 14. PSP-MIL-53 showed ion adsorption capacities 1.69, 2.73, and 2.88 mmol $g^{-1}$ at a feed flux of 100 LMH, when dealing with 1,000, 10,000, and 35,000 ppm salt solutions, respectively. The relevant fresh water produced were 82.4, 7.1, and 2.5 mL $g^{-1}$. Accordingly, the volume of sorbent exhaustion was 88.5, 13.8, and 5.4 mL $g^{-1}$, respectively Based on these preliminary results, the ion adsorption loading and the fresh water volume at other NaCl concentration were calculated, as shown in Supplementary Fig. 15. It is found that 82.5, 28.4, 18.9, 14.6, 12.1, 8.9, 7.1, 4.1, and 2.5 mL $g^{-1}$ of fresh water were produced by PSP-MIL-53 when dealing with 1,000, 2,000, 3,000, 4,000, 5,000, 7,500, 10,000, 20,000, and 35,000 ppm NaCl solutions, respectively.

The amount of fresh water needed for regeneration of PSP-MIL-53 was determined to be 1.5 mL $g^{-1}$. Supplementary Fig. 17 shows the mobility of PSP-MIL-53 with different amounts of water. PSP-MIL-53 with 1 mL $g^{-1}$ of water looked like moist soil, while the water could not be filtered out. 2.5 mL $g^{-1}$ of water endowed the PSP-MIL-53 suspension with good mobility for regeneration. Due to the reserve of water within adsorbent (1 mL $g^{-1}$) during the adsorption process, an extra 1.5 mL $g^{-1}$ of water should be added for regeneration. Therefore, excluding 1.5 mL $g^{-1}$ fresh water for regeneration, 81.0, 5.6, and 1 mL $g^{-1}$ of fresh water could be produced when treating 1,000, 10,000, and 35,000 ppm NaCl solutions with PSP-MIL-53, respectively.

**Supplementary Note 6 | Desalination of synthetic brackish water and synthetic seawater by PSP-MIL-53**

Synthetic brackish water and seawater were prepared and desalted by PSP-MIL-53 under dark in the single-column setup, individually. The feed solution flux during the desalination process was ~100 LMH.

The compositions of synthetic brackish water are listed in Table 1, with a salt concentration of 2,233 ppm, and a pH of 7.8. 0.13 g of PSP-MIL-53 was packed in the single-column setup with a packing density of 607 g $L^{-1}$. 4.50 mL of desalted water was collected for analysis (ALS Environmental, Melbourne, Australia). The results showed that the PSP-MIL-53 had an ion adsorption loading of 1.06 mmol $g^{-1}$, and 1.33 meq $g^{-1}$. Specifically, it adsorbed 0.45 mmol $g^{-1}$ of $Cl^-$, 0.082 mmol $g^{-1}$ of $HCO_3^-$, 0 mmol $g^{-1}$ of $NO_3^-$, 0.031 mmol $g^{-1}$ of $SO_4^{2-}$, 0.26 mmol $g^{-1}$ of $Na^+$, 0.11 mmol $g^{-1}$ of $Ca^{2+}$, 0.13 mmol $g^{-1}$ of $Mg^{2+}$. Accordingly, 23.4 mL of fresh water (<600 ppm) could be produced by each gram of PSP-MIL-53.

As for the desalination of synthetic seawater with a pH of 8.3, 0.63 g of PSP-MIL-53 was packed in the single-column. 1.71 mL of desalted seawater was collected for analysis. The 35,000 ppm synthetic seawater was desalted to be 6,106 ppm, while 2.3 mL of fresh water could be produced by each gram of PSP-MIL-53. PSP-MIL-53 exhibited a salt adsorption loading of 2.47 mmol $g^{-1}$ and 2.66 meq $g^{-1}$.

In this study, salt solution, synthetic brackish water and synthetic seawater were used to study the adsorption performance of PSP-MIL-53. Ions could be efficiently removed by PSP-MIL-53. However, the real water samples contain ions and other contaminants, such as organics and proteins. MOF particles have been widely developed to remove organics from water[13]. In terms of the adsorption of contaminants by PSP-MIL-53, it can be due to the wettability and charge adsorption. However, because of the 8.5 Å pore size of PSP-MIL-53, contaminants with size larger than 8.5 Å could not access the adsorption sites inside MOF framework. Therefore, many of the contaminants with large size (>8.5 Å) may be left in the desalted water. To treat real water samples with other contaminant, other process, such as advanced oxidation process or membrane process, may need to use to remove organic contaminants.

## Supplementary Note 7 | A two-bed system designed for brackish water desalination and estimation of energy consumption

### *7.1. Parameters of a simple packed column*

According to our results for the desalting of synthetic brackish water (2,233 ppm) in the single-column setup, each gram of PSP-MIL-53 could produce 23.4 mL fresh water with a salt concentration down to 600 ppm and even less. Hereafter, we intend to conduct a simple energy/mass balance for a virtual fresh water yield of 10 $m^3$ per column, per single cycle. By

doing this, we further aim to compare the energy consumption of our process with those processes well established in the industry.

Based on the facts that the ionic amount in the synthetic brackish water feedstock tallies 65.46 mmol $L^{-1}$, the ionic amount needed to be adsorbed is 47.88 mmol $L^{-1}$ (1,663 ppm), and the adsorption loading of PSP-MIL-53 is 1.06 mmol $g^{-1}$, the amount of PSP-MIL-53 ($W_{PSP\text{-}MIL\text{-}53}$, kg) can be determined as 451.7 kg, as shown by the equation below.

$$W_{PSP\text{-}MIL\text{-}53}=\frac{47.88\times10{,}000}{1.06\times10{,}00}=451.70 \text{ kg}$$

In this study, the packing density of adsorbents is 607 g $L^{-1}$ in the single-column setup. Assuming a packing density of the packed bed is 607 g $L^{-1}$ in this calculation, the volume of adsorbent ($V_{PSP\text{-}MIL\text{-}53}$, $m^3$) is

$$V_{PSP\text{-}MIL\text{-}53}=\frac{451.70}{607}=0.74 \text{ m}^3$$

The spent PSP-MIL-53 is regenerated with visible light irradiation. In order to better transfer light within PSP-MIL-53, the same volume of glass beads with the adsorbent was assumed here. The particles composed of PSP-MIL-53 and glass beads will have an identical average diameter of 200 μm. Consequently, the total volume of adsorbent and glass beads ($V_{total}$, $m^3$) is

$$V_{total}=0.74\times2=1.48 \text{ m}^3$$

We choose a bed height $L$ of 2 m, thus, the bed diameter ($d_{bed}$, m) is

$$d_{bed}=\sqrt{\frac{4V_{total}}{\pi L}}=\sqrt{\frac{4\times1.48}{\pi\times2}}=0.97 \text{ m}$$

As the batch adsorption results for an established adsorption equilibrium duration of 30 min, the filtration velocity ($u$, m $h^{-1}$) is

$$u = \frac{2}{0.5} = 4 \text{ m h}^{-1}$$

The volumetric flow rate $f$ ($m^3$ $h^{-1}$) is thus determined as

$$f = 4\times\pi\times(0.97\div2)\text{^}2 = 2.96 \text{ m}^3 \text{ h}^{-1}$$

Accordingly, the time requested for a single adsorption batch to complete ($t_{salt\ adsorp.}$, h) is

$$t_{salt\ adsorp.} = \frac{10}{2.96} = 3.38 \text{ h}$$

As for the regeneration of used adsorbent, it is found that 1.5 mL of fresh water is needed for each gram of PSP-MIL-53. Moreover, another 451.70 L of fresh water is necessary to rinse the adsorbent bed before the start of another cycle. Thus, the volume of water ($V_{regen.}$, $m^3$) needed for regeneration is

$$V_{regen.} = \frac{1.5\times451.70}{1{,}000} + \frac{451.70}{1{,}000} = 1.13 \text{ m}^3$$

To accommodate the installation of liquid distribution plates in a commercial packed bed, the column height is extended up to around 3.5 m. Such an approach also means our energy consumption estimation conservatively and even more than the actual energy required. According to the new bed height, the eluted brine concentration ($C_{brine}$, ppm) is

$$C_{brine} = \frac{1{,}663\times10\times1{,}000}{1.13\times1{,}000} = 14{,}716 \text{ ppm}$$

According to the volumetric flow rate of feed brackish water, a pump with a flow rate of 3 $m^3$ $h^{-1}$ will be chosen for both the desalination and regeneration process. Thus, the time needed for one regeneration process ($t_{regen.}$, h) including the time for pumping, light irradiation (0.5 h), draining, and rinsing that can be estimated as

$$t_{regen.} = \frac{1.5\times451.70}{3\times1{,}000} + 0.5 + \frac{1.5\times451.70}{3\times1{,}000} + \frac{451.70}{3\times1{,}000} = 1.10 \text{ h}$$

These results are summarized in Supplementary Table 5.

*7.2. Design of a two-bed system*

The desalination process includes salt adsorption process under dark condition and regeneration process under visible light irradiation. A two-bed system for photocontrol brackish water desalination under dark and visible light is thus designed and illustrated in Supplementary Fig. 20. The two beds will be operated alternately. That is, at each time only one single bed is used for the adsorption. Once the adsorption bed is saturated, the brackish water feedstock is fed into another bed to continue the treatment, while the saturated bed is subjected to the regeneration conditions, as optimized in our study. Such a design is also common in the industry.

According to Supplementary Note 7.1, the salt adsorption process takes 3.38 h, while the regeneration process only takes 1.10 h. One pump is installed above the two columns to supply brackish water at a pressure required for the optimum operation and to overcome the pressure drop across the bed. Regarding the fresh water supply for the bed regeneration, one pump is designed for the two beds, since each time only a single bed is in operation. There is a gate on top of each column. The gate is closed to achieve dark condition, while opens for visible light irradiation. We assume an irradiation duration of 12 h with sunlight in the daytime and the same irradiation duration in the night when lamps are used to provide the visible light illumination.

Therefore, the number of adsorption cycles in a day ($n_{cycles}$) is

$$n_{cycles} = \frac{24}{3.38} = 7.10$$

The net capacity ($m^3$) of the two-bed system excluding the amount of fresh water needed for regeneration is further estimated as

$$Net\ capacity\ = 7.10\times10 - 7.10\times1.13 = 62.98\ m^3 \cdot d^{-1}$$

*7.3. Energy calculation based on the two-bed system*

Based on the design of the two-bed desalination system in Supplementary Fig. 20 and in Supplementary Note 7.2, the energy consumption of the process including the energy of pumping and lighting can be estimated. The criteria for selection of pumps and lamps are further detailed below.

*7.3.1. Pumps*

The void fraction ($\varepsilon$) of the bed is

$$\varepsilon = \frac{V\text{-}V_P}{V} = \frac{1\text{-}0.607}{1} = 0.393$$

Here, the bed density is 607 g $L^{-1}$. The density of MIL-53 is 0.98 g $cm^{-3}$ [1]. After adding 22.5 wt.% of PSP, we further assume the density of PSP-MIL-53 to be ~1 g $cm^{-3}$.

The pressure drop of the adsorbents is calculated according to the Ergun equation:

$$\Delta p = 150\frac{(1\text{-}\varepsilon)^2}{\varepsilon^3}\frac{\mu \cdot u_s \cdot L}{{d_p}^2} + 1.75\frac{(1\text{-}\varepsilon)}{\varepsilon^3}\frac{\rho \cdot L \cdot {u_s}^2}{d_p}$$

where $\varepsilon$ is the void fraction of the bed, which is 0.393. $\mu$ is the viscosity of 2,233 ppm (0.033 mol $kg^{-1}$) brackish water, which is $8.93\times10^{-4}$ Pa s at 25°C [14]. $u_s$ is the superficial velocity of brackish water, which is $u_s$ = 4÷0.393÷3600=0.0028 m $s^{-1}$. The bed height $L$ is 2 m. $\rho$ is the density of PSP-MIL-53, which is estimated to be ~1,000 kg $m^{-3}$. $d_p$ (m) is the diameter of PSP-MIL-53. The SEM image has suggested that PSP-MIL-53 particles were aggregates (20-30 μm)

of small particles. Concerning the pressure drop across the bed, the size of PSP-MIL-53 aggregates are further increased (crosslinked) to reach ~200 μm for practical application. The small as-synthesized particles can be readily used to fabricated into hierarchical porous beads using commercially available techniques such as spray drying[15]. Such a size is also the same as the glass beads. Therefore, the pressure drop of this packing bed ($\Delta p$, Pa or bar) is

$$\Delta p = \frac{150\times(1-0.393)^2}{0.393^3}\frac{8.93\times10^{-4}\times0.0028\times2}{(200\times10^{-6})^2} + \frac{1.75\times(1-0.393)}{0.393^3}\frac{1{,}000\times2\times0.0028^2}{200\times10^{-6}} = 107823 \text{ Pa} = 1.08 \text{ bar}$$

Thus, the pumps are selected to provide a volumetric flow rate of 3 m $h^{-1}$, to overcome the pressure of 1.08 bar, and to have a discharge head of >3.5 m (column height). Accordingly, we searched for the pump catalogue of Kolmeks (Finland), and found a suitable one (AP-15/2 OP-741 N12, impeller size $\Phi$=80 mm) that could afford the requirements. AP-15/2 OP-741 N12 can be used in circulation, pressure booster and transfer pumps for water. This pump can provide up to 10 bar of operating pressure, and works at −15 to 100 °C. According to the parametric curves of this pump, the discharge head and the electrical power respectively reach 7.3 m and 0.19 kW for a water flow rate of 3 m $h^{-1}$. For the two pumps required here, the specific energy consumption of pumping ($E_{pumps}$, kWh $m^{-3}$) is determined as

$$E_{pumps} = \frac{0.19\times24+0.19\times1.10\times7.10}{62.98} = 0.096 \text{ kWh}\cdot\text{m}^{-3}$$

*7.3.2. Lights*

In this calculation, we assume that there are 12 h daytime and 12 h night time in each single day. In the daytime, sunlight is used as the visible light source. According to our study, PSP-MIL-53 could be regenerated within 4 min under one sun (1000 W $m^{-2}$) illumination, and 30 min under 0.1 sun illumination. To ensure a sufficient regeneration during the daytime, the

regeneration process is set to be 30 min, and the total time for regeneration including the pumping and rinsing time is determined to be 1.10 h, as detailed in our previous calculation.

In the night time, the visible light source is provided by lamps. Here, we chose the ceramic metal halide discharge reflector lamp (MASTERColour LDBE_CDM-R-E_0002, Philips) as the visible light source. According to the beam diagram, this lamp can provide visible light with an illuminance of 14130 lux and a spot diameter of 0.35 m, in 2 m height from the lamp. The illuminance of 14130 lux falls within the range of full daylight (10,000-25,000 lux), which is sufficient for the visible light regeneration process. In order to fully cover the bed area, the numbers of lamps ($n_{lamps}$) needed is

$$n_{lamps}=\frac{\pi\times(0.97\div2)^2}{\pi\times(0.35\div2)^2}=7.7\approx8$$

The energy consumption of this lamp is 43 kWh per 1000 h, and the lamps are on in the night time cycles (3.55 cycles in night, 0.5 h each cycle). Therefore, the specific energy consumption of the lighting ($E_{lights}$, kWh $m^{-3}$) is

$$E_{lights}=\frac{0.043\times8\times0.5\times3.55}{62.98}=0.010\ \text{kWh}\cdot\text{m}^{-3}$$

*7.3.3. Total specific energy consumption*

When sunlight and room lighting are used for the visible light regeneration process, the total specific energy consumption ($E$, kWh $m^{-3}$) including the energy consumption of pumping and lighting are shown below

$$E=E_{pumps}+E_{lights}=0.096+0.010=0.11\ \text{kWh}\cdot\text{m}^{-3}=0.11\ \text{Wh}\cdot\text{L}^{-1}$$

The above results are summarized in Supplementary Table 6.

When using room lighting for the whole regeneration process, the total specific energy consumption is increased to be

$$E=E_{pumps}+2\times E_{lights}=0.096+0.020=\ 0.21\ \text{kWh}\cdot\text{m}^{-3}=\ 0.21\ \text{Wh}\cdot\text{L}^{-1}$$

## SUPPLEMENTARY FIGURES

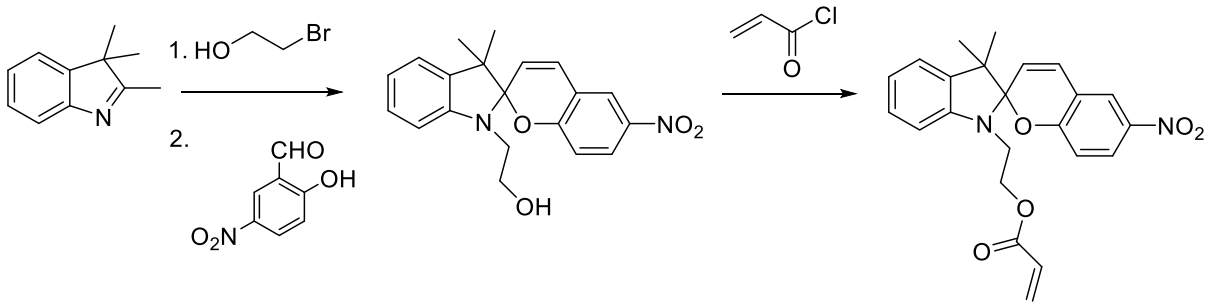


**Supplementary Fig. 1 |** Synthesis procedures of spiropyran acrylate.

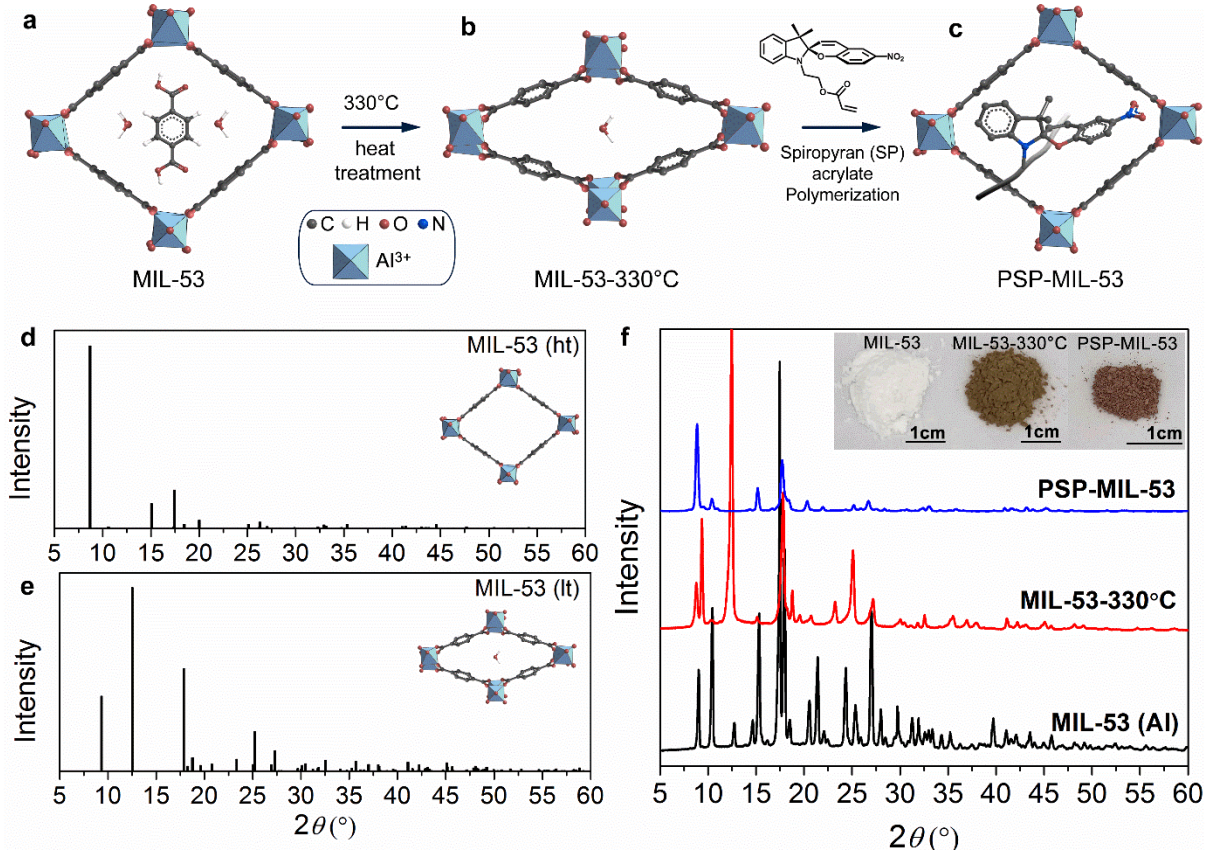


**Supplementary Fig. 2 | Synthesis and characterization of PSP-MIL-53.** (**a-c**) Synthesis of PSP-MIL-53. The (a) as-prepared MIL-53 is emptied pore by heat treatment at 330°C to obtain (b) MIL-53-330°C before introduction of SP. (**d-f**) The significant breathing effect of MIL-53 upon emptying and filling pores. (d) Simulated XRD pattern of MIL-53 (ht) with empty pores. (e) Simulated XRD pattern of MIL-53 (lt) partially filled with water molecules. (f) XRD patterns of as-prepared MIL-53, MIL-53-330°C, and PSP-MIL-53. The inset of (f) are the optical images of MIL-53, MIL-53-330°C, and PSP-MIL-53.

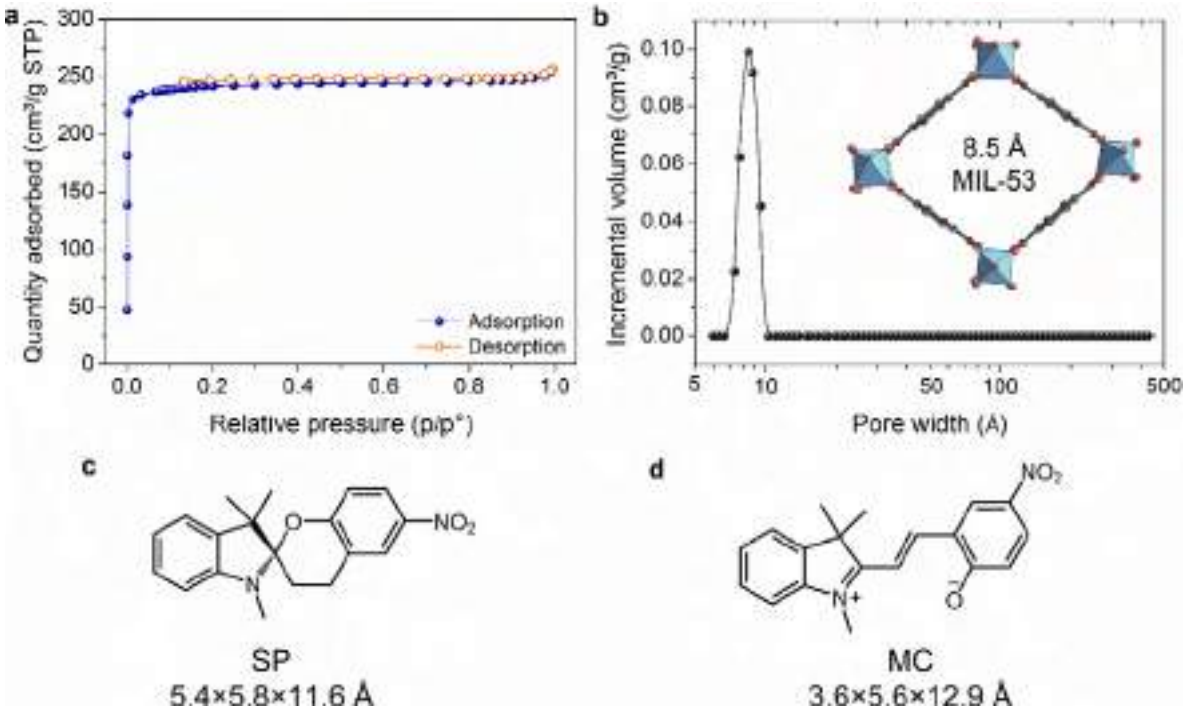


**Supplementary Fig. 3 |** (**a**) $N_2$ adsorption-desorption isotherm of MIL-53. The obtained MIL-53 has a BET surface area of 874.5 $m^2$ $g^{-1}$, and a Langmuir surface area of 1077.0 $m^2$ $g^{-1}$. (**b**) Pore width distribution of MIL-53. Molecular structures and sizes of (**c**) spiropyran (SP) and (**d**) merocyanine (MC) determined by Chem3D 17.0.

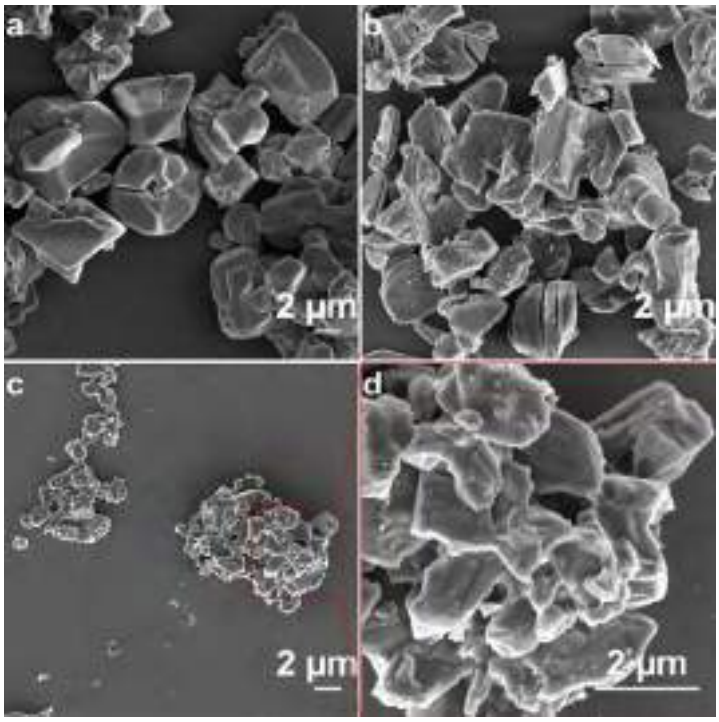


**Supplementary Fig. 4 |** SEM images of the morphology of (**a**) as-prepared MIL-53, (**b**) MIL-53-330°C, and (c-d) PSP-MIL-53.

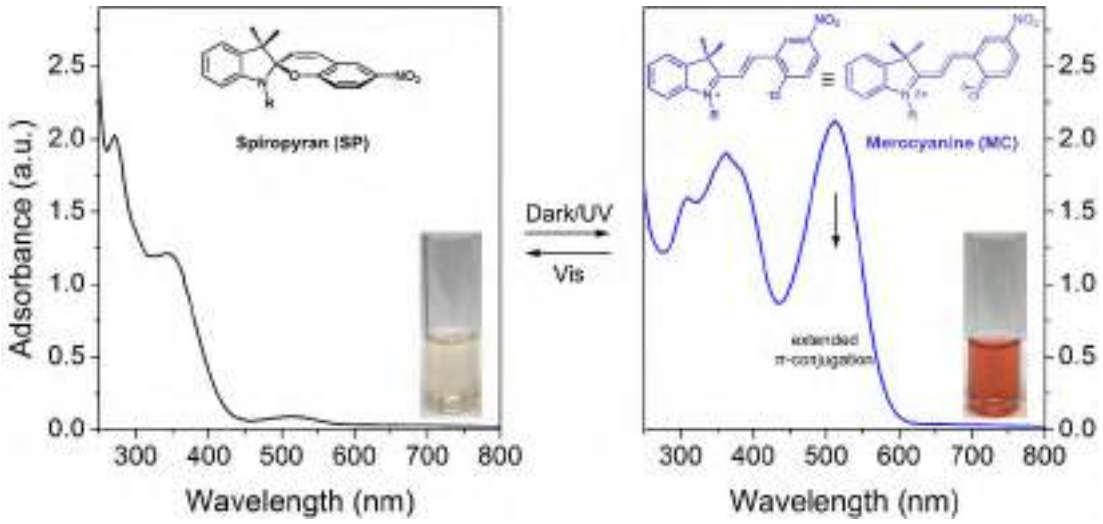


**Supplementary Fig. 5 | UV-Vis spectra of SP and MC in 10,000 ppm NaCl solution.** The formation of strong peak at 512 nm is due to the extended π-conjugation between the indolium and chromene moieties of merocyanine.

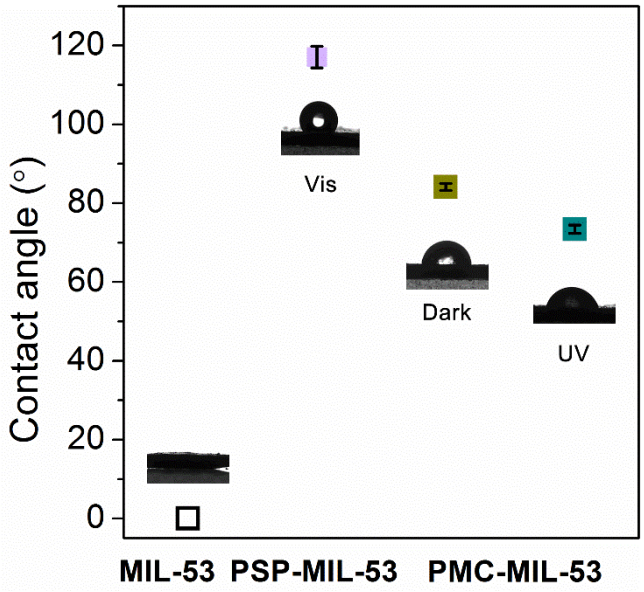


**Supplementary Fig. 6 |** Water contact angle of MIL-53-330°C, PSP-MIL-53, and PMC-MIL-53.

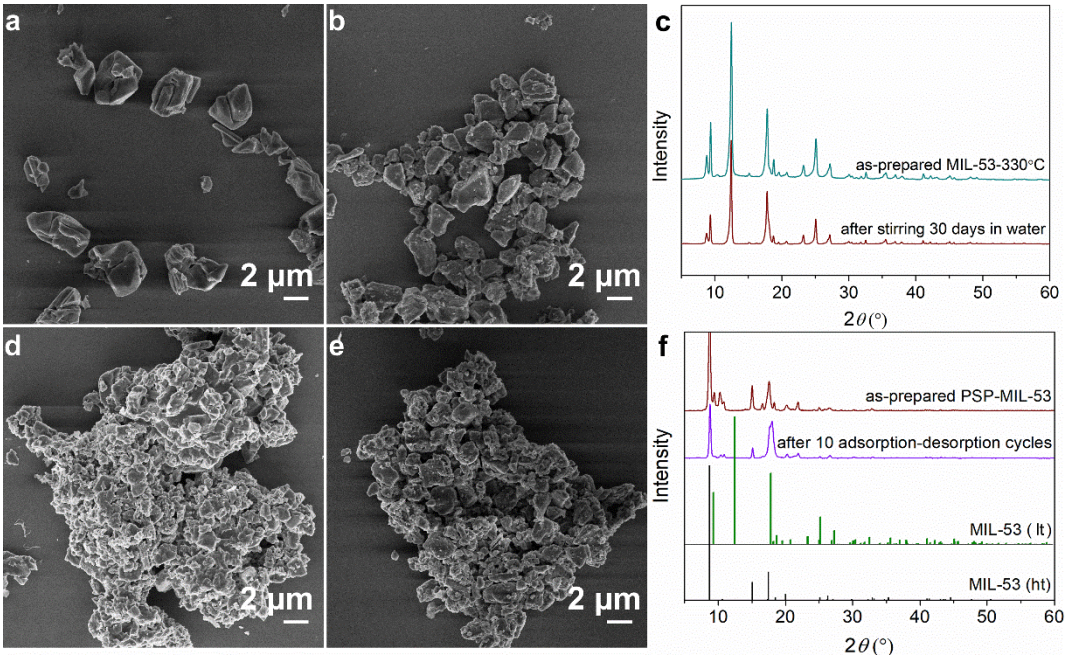


**Supplementary Fig. 7 | Stability of MIL-53-330°C and PSP-MIL-53.** SEM images of (**a**) as-prepared MIL-53-330°C and (**b**) those after stirring in water for 30 days. (**c**) XRD patterns of MIL-53-330°C before and after stirring in water for 30 days. SEM images of (**d**) as-prepared PSP-MIL-53 and (**e**) those after 10 adsorption-desorption cycles. (**f**) XRD patterns of PSP-MIL-53 before and after 10 adsorption cycles, and the simulated XRD pattern of MIL-53 (lt) with contracted framework and MIL-53 (ht) with expanded framework.

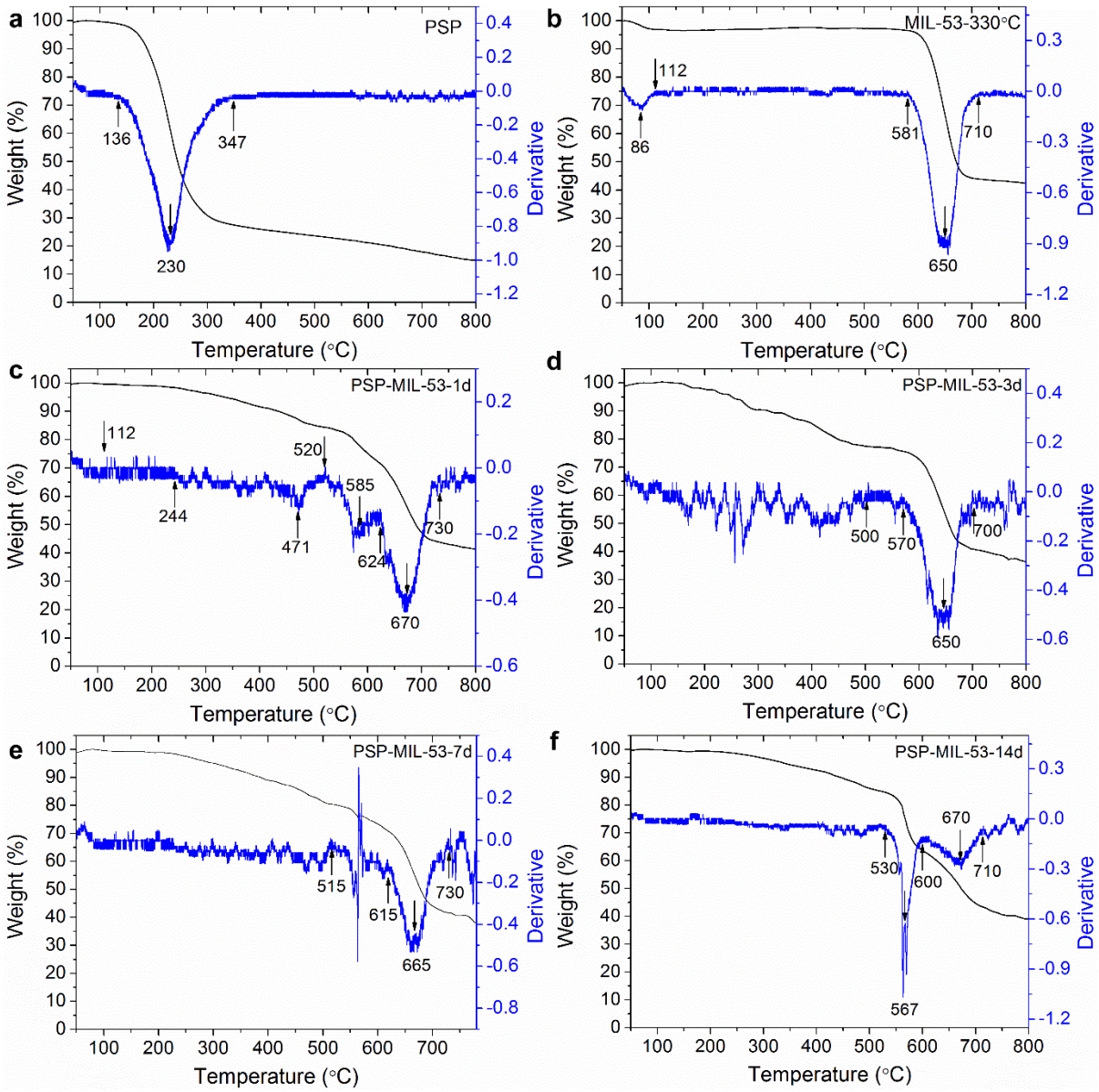


**Supplementary Fig. 8 |** Thermogravimetric analysis curves and the relevant derivative of (**a**) PSP, (**b**) MIL-53-330°C, (**c**) PSP-MIL-53-1d, (**d**) PSP-MIL-53-3d, (**e**) PSP-MIL-53-7d, and (**f**) PSP-MIL-53-14d. The TGA was conducted in Air flow.

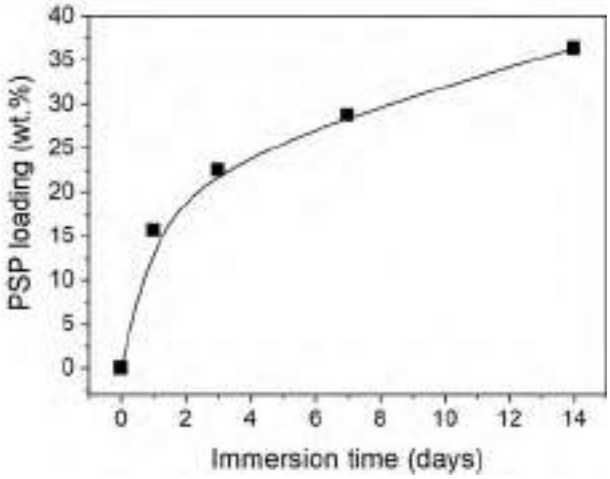


**Supplementary Fig. 9 |** The effect of immersion days before polymerization on the PSP loading of PSP-MIL-53. The calcined MIL-53, spiropyran acrylate, and AIBN were added into ethanol. The suspension was stirred at room temperature for 1, 3, 7, and 14 days (immersion days) before allowing evaporation of ethanol in fume hood until visibly dried. Then, the sample was polymerized in an oven at 70 °C.

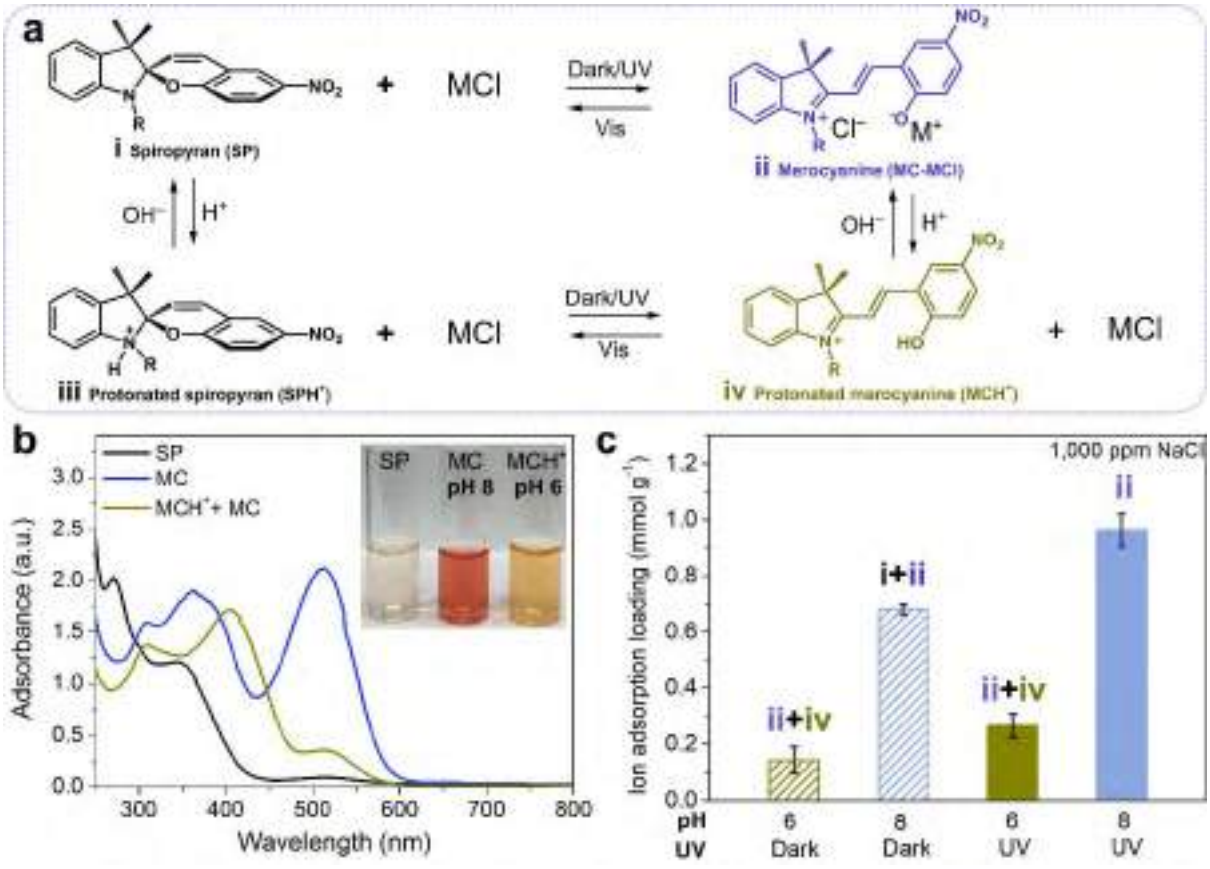


**Supplementary Fig. 10 | The significant effect of pH on the ion adsorption loading of spiropyran.** (**a**) The mechanism of pH influence on the MCl adsorption. (**b**) UV-Vis spectra of SP, activated MC (pH 8), and $MCH^+$ (pH 6) measured in 10,000 ppm NaCl aqueous solution. (**c**) The effect of pH and activation source (Dark/UV 254 nm) on the ion adsorption loading of PSP-MIL-53.

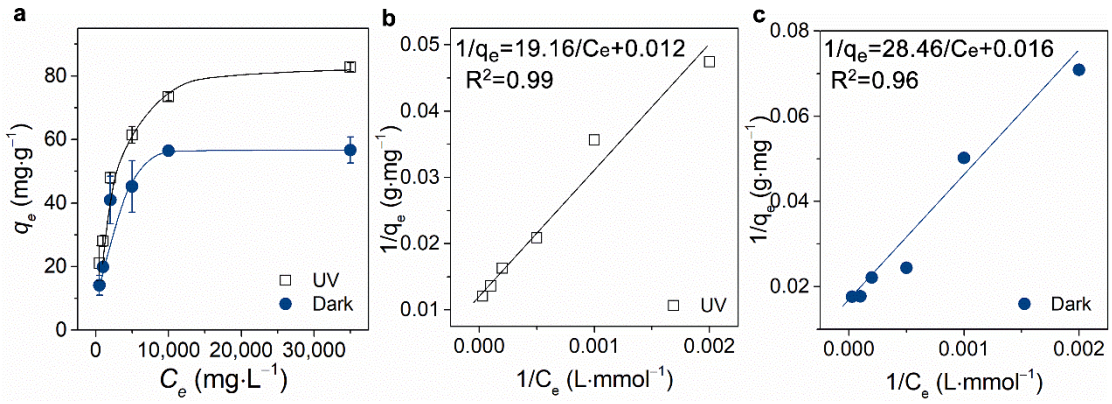


**Supplementary Fig. 11** | NaCl adsorption isotherms of PSP-MIL-53. **a,** Dependence of ion adsorption loading of PSP-MIL-53 on NaCl concentration under UV and dark condition. **b-c,** The adsorption isotherm of PSP-MIL-53 measured under UV and dark condition well fitted with Langmiur model. Supplementary Fig. 11a is the same as Fig. 2e in the manuscript.

The NaCl uptake isotherms with error bars have been quantified using batch uptake experiments under UV light and dark condition, as shown in Supplementary Fig. 11. In order to fit the adsorption data into the isotherm models, the title of x axis has been modified to $C_e$ (mg L$^{-1}$), and the title of y axis has been changed to $q_e$ (mg g$^{-1}$) in Supplementary Fig. 11a. $C_e$ is the equilibrium NaCl concentration, and $q_e$ is the NaCl adsorption loading. Then, the results of ion uptake isotherms under UV and dark condition have been fitted into three isotherm models, including Langmuir, Freundlich, and Tempkin model. As shown in Supplementary Table 2 and Supplementary Fig. 11b-c, the adsorption data of PSP-MIL-53 were best fitted with Langmuir model among the three models, with $R^2 \geqslant 0.96$. Therefore, the Langmuir model well describes the adsorption of ions into PSP-MIL-53 adsorbent.

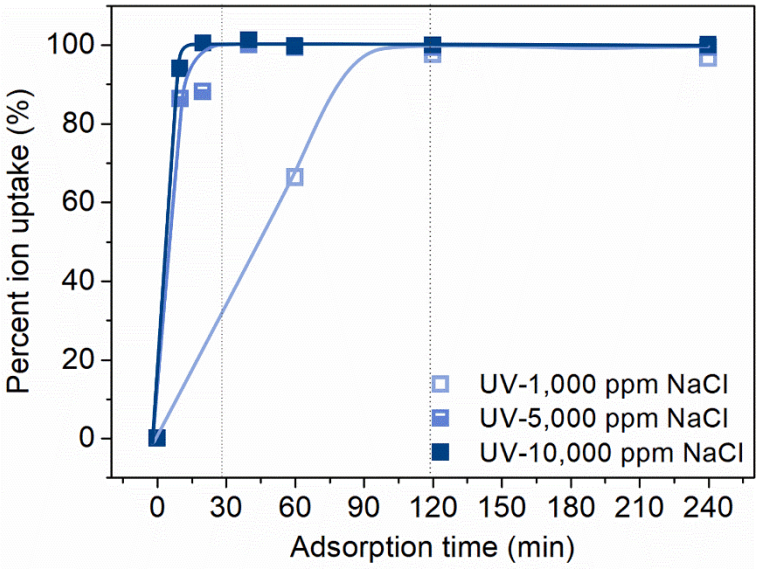


**Supplementary Fig. 12 | Adsorption kinetic of PSP-MIL-53.** The adsorption kinetics of PSP-MIL-53 was measured under UV light irradiation in 1,000 ppm NaCl solution (□), 5,000 ppm NaCl solution (▬), and 10,000 ppm NaCl solution (■). Due to the different ion adsorption loading of PSP-MIL-53 in different salt concentrations, the ion adsorption loading at each concentration was normalized to percent ion uptake for better comparison.

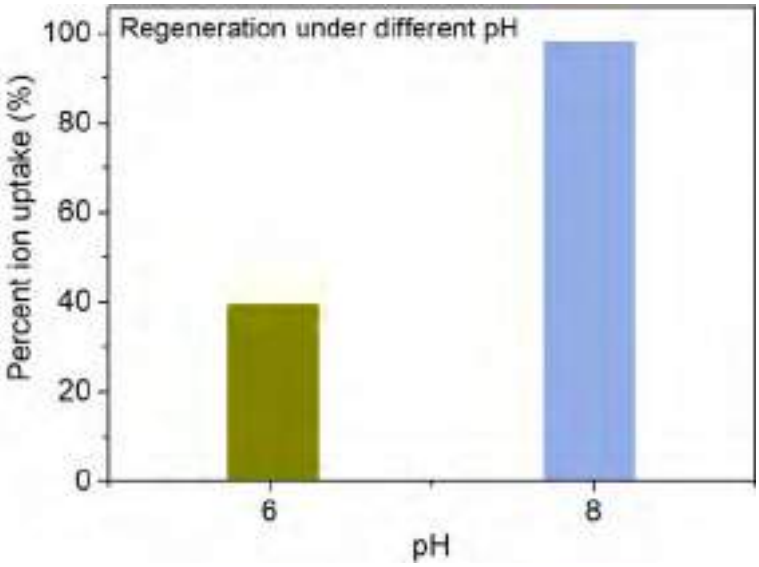


**Supplementary Fig. 13 | The effect of pH on the regeneration of PSP-MIL-53 under visible light.** The pH of the water used for regeneration was adjusted by HCl (pH 2) and NaOH (pH 12) solutions. PSP-MIL-53 was used to adsorb ions in 1,000 ppm NaCl solution, showing adsorption loading $q_1$. Then, the PSP-MIL-53-NaCl was regenerated in water with a pH of 6 and 8, respectively. Thereafter, the regenerated was used to adsorb ions in 1,000 ppm NaCl solution again, showing adsorption loading $q_2$. The percent ion uptake (%) are calculated by the follow equation:

$$Percent\ ion\ uptake\ (\%) = \frac{q_2}{q_1} \times 100$$

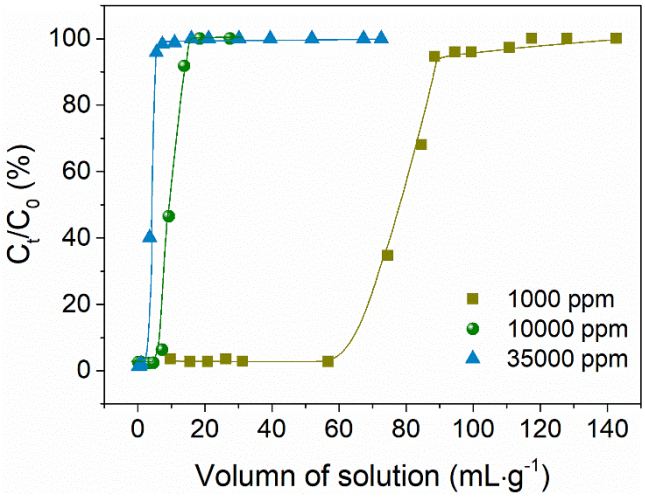


**Supplementary Fig. 14 |** The breakthrough curves of PSP-MIL-53 measured with NaCl concentrations of 1000, 10,000, and 35,000 ppm. The inner diameter of column is 0.6 cm, bed depth is 0.85 cm, and the bed density is 607 g L$^{-1}$. The solution filtration flux is ~100 LMH.

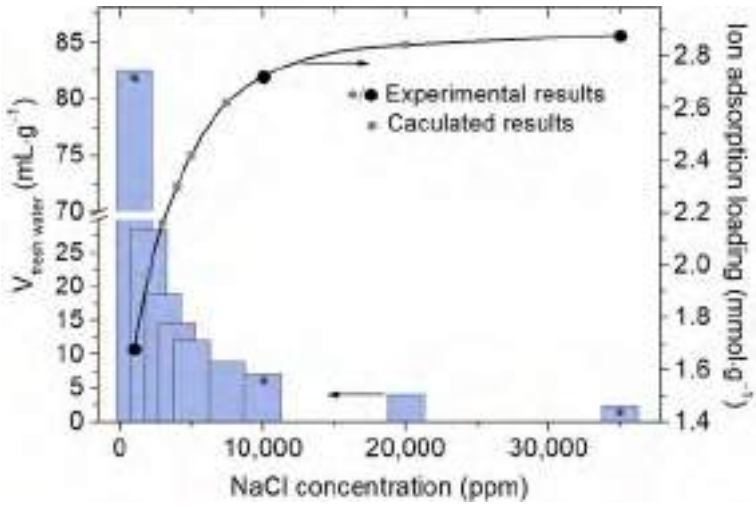


**Supplementary Fig. 15 |** The volume of fresh water obtained and the relevant ion adsorption loading upon increasing NaCl concentration. The results were calculated based on the experimental data marked as */●.

The ion adsorption loadings obtained in the single-column tests were 1.68, 2.72, and 2.88 mmol g$^{-1}$ at the NaCl concentration of 1,000, 10,000, and 35,000 ppm, respectively. These results were fitted into the Langmuir model, resulting in a relation of $q_e = \frac{0.230C_e}{(1+0.0785C_e)}$ ($R^2$=0.999). The ion adsorption loadings at different concentrations were calculated accordingly.

Then, the volume of fresh water produced at different salt concentration can be calculated by

$$V\ (mL \cdot g^{-1}) = \frac{q_e \cdot M_s \cdot r_b}{n \cdot (C\text{-}600)}$$

where $q_e$ (mmol $g^{-1}$) is the ion adsorption loading at different concentration $C$ (mg $L^{-1}$), $Ms$ (g $mol^{-1}$) is the molecular weight of NaCl, $n$ is the number of cation and anion of NaCl, which equals to 2. ($C-600$) (mg $L^{-1}$) means the concentration of salt solution should be adsorbed by the adsorbent. However, because the solution cut off is at a concentration of 600 ppm, which indicates the obtained fresh water with a concentration lower than 600 ppm. Furthermore, the actual ion adsorption loading of PSP-MIL-53 at the concentration of 600 ppm has not reached the calculated value. Therefore, an empirical coefficient $r_b$ is used to correct the volume of fresh water produced based on the results of breakthrough curves. $r_b$ equals to 0.67, 0.84, and 0.9998 when the NaCl concentration is 1,000, 10,000, and 35,000 ppm. These results were fitted into curve by OriginPro, showing an equation of $r_b$=1.05-0.40*0.99994$^C$ ($R^2$=0.998), where $C$ (mg $L^{-1}$) is the salt concentration.

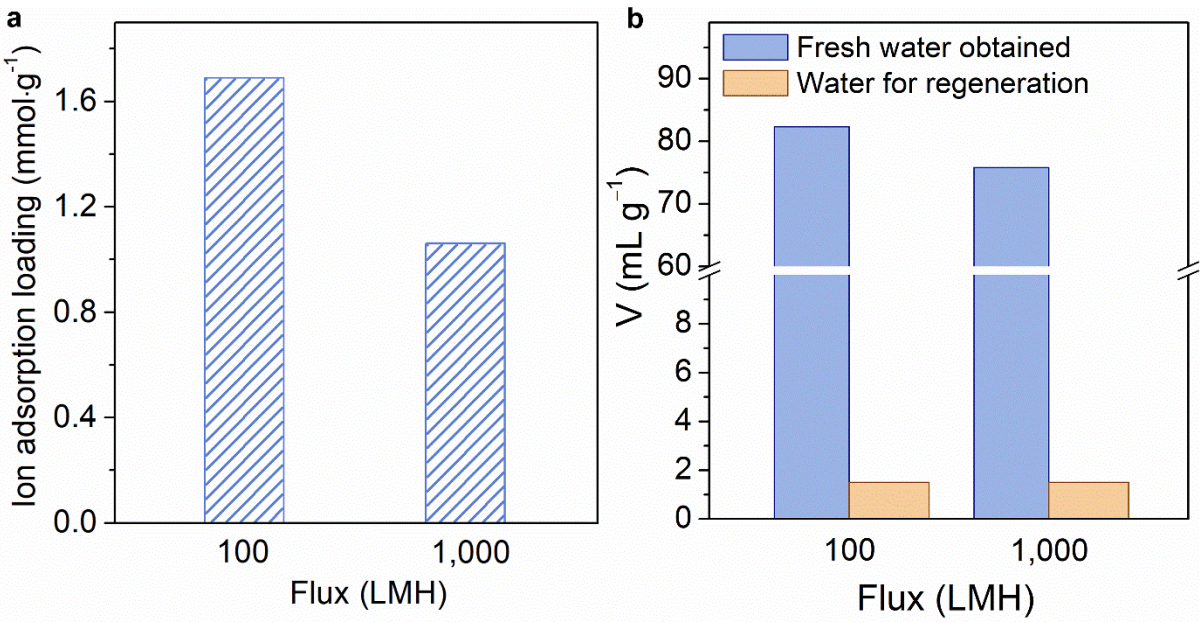


**Supplementary Fig. 16 | Single-column adsorption performance of PSP-MIL-53.** (**a**) Ion adsorption loading of PSP-MIL-53 with feed solution flux of 100 and 1,000 LMH, respectively. The ion adsorption loading at 1000 LMH is 1.06 mmol $g^{-1}$. (**b**) The amount of fresh water obtained with flux of 100 and 1,000 LMH, and the fresh water needed for the regeneration of PSP-MIL-53. 1,000 ppm NaCl solution was used as feed.

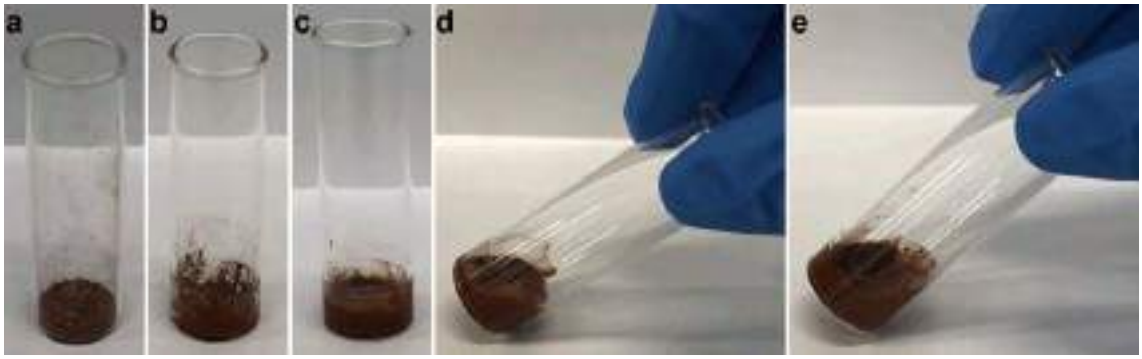


**Supplementary Fig. 17 |** The mobility of PSP-MIL-53 with different amounts of water: (**a**) 0 mL $g^{-1}$, (**b**) 1 mL $g^{-1}$, (**c**) 2 mL $g^{-1}$, (**d**) 2.5 mL $g^{-1}$, (**e**) 3 mL $g^{-1}$. PSP-MIL-53 with 1 mL $g^{-1}$ of water looks like moisturized granular soil. When the water amount increases to 2 mL $g^{-1}$, it becomes a viscous suspension. The PSP-MIL-53 with 2.5 or 3 mL $g^{-1}$ water shows good flowability.

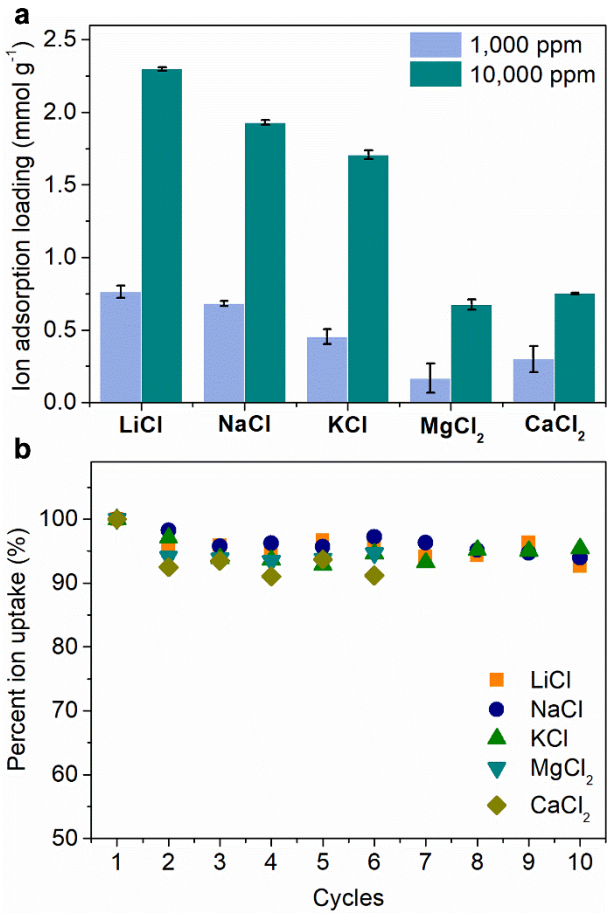


**Supplementary Fig. 18 | Adsorption of multiple salts by PSP-MIL-53 and their cycling performance.** (**a**) The ion adsorption loading of different salts (LiCl, NaCl, KCl, $MgCl_2$, and $CaCl_2$). When the salt concentration was 1,000 ppm, the relevant ion adsorption loading of LiCl, NaCl, and KCl dropped to 0.76, 0.68, and 0.45 mmol $g^{-1}$, while that of $MgCl_2$ and $CaCl_2$ were 0.17 and 0.30 mmol $g^{-1}$, respectively. (**b**) Cycling performance of PSP-MIL-53. 10,000 ppm salt solution was used for the characterization.

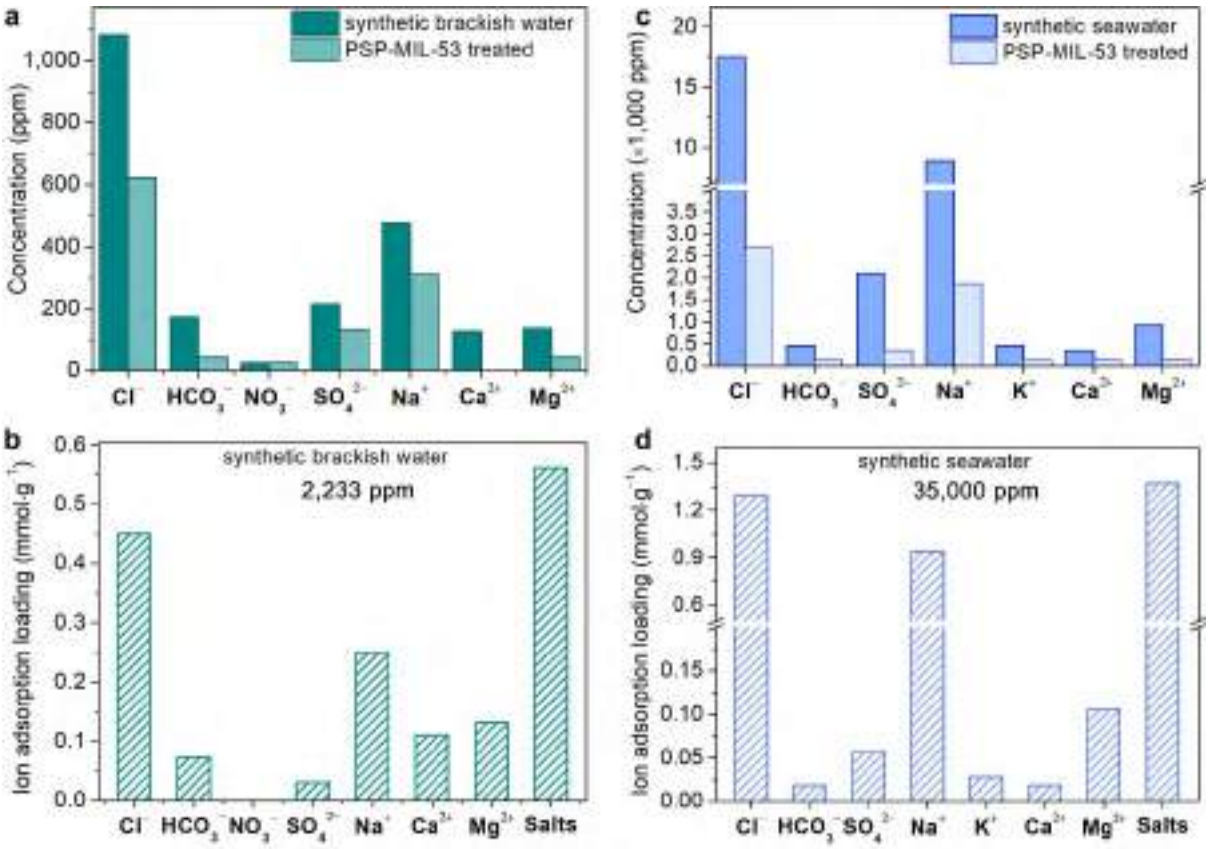


**Supplementary Fig. 19 | Desalination of synthetic brackish water and synthetic seawater by PSP-MIL-53 in single-column setup.** (**a**) The ion concentrations of the synthetic brackish water before and after adsorption. (**b**) The ion adsorption loading of PSP-MIL-53 for desalination of synthetic brackish water. (**c**) The ion concentrations of the synthetic seawater before and after adsorption. (**d**) The ion adsorption loading of PSP-MIL-53 for desalination of synthetic seawater.

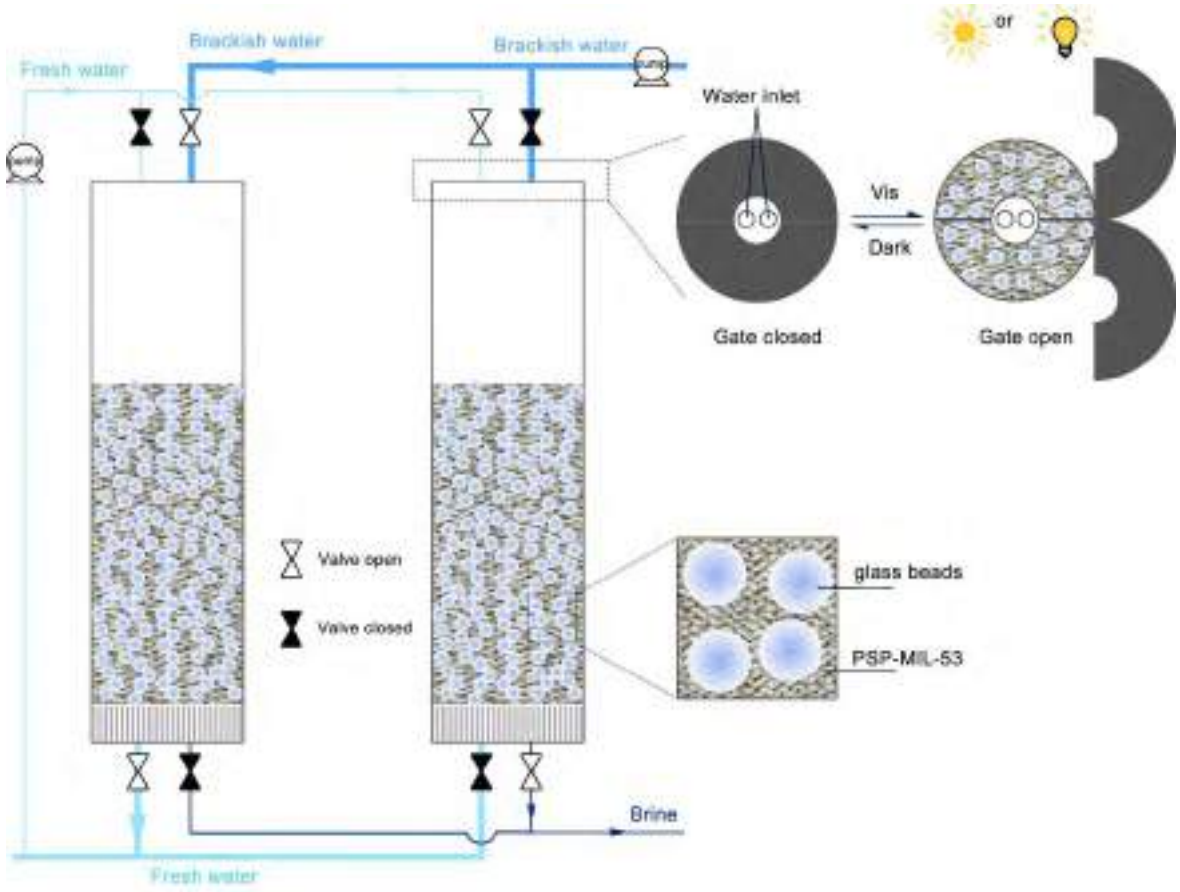


**Supplementary Fig. 20 | Schematic illustration of a two-bed system for brackish water desalination under dark and visible light.** This column is designed according to the result of desalting synthetic brackish water (2,233 ppm) in this study. The gate located on top of the column could be open (Vis) and closed (dark). Salt removal process is performed with gate closed, while the regeneration process is running with gate open for visible light irradiation. Glass beads are mixed with PSP-MIL-53 to transmit visible light for regeneration[16,17]. Please see Supplementary Table 5 and Supplementary Table 6 for detailed parameters of the column and the desalination process.

## SUPPLEMENTARY TABLES

**Supplementary Table 1 |** The pH values of natural brackish water and seawater.[a]

| No. | Salt water sources | Salinity (ppm) | pH | Ref. |
|---|---|---|---|---|
| **1** | Underground water in the centre of Morocco | 2,208 | 7.9 | [8] |
| **2** | Surface waters of Küçükçekmece Lake | 596-1,020 | 7.0-8.4 | [18] |
| **3** | Underground water of Borj-Cédria | 5,424 | 7.2 | [19] |
| **4** | Lake Vargsundet | ~2,000 | 8.9-9.4 | [20] |
| **5** | Ground water in Gaza strip | ~700-3,000 | 6.0-8.0, mostly >7.0 | [21] |
| **6** | Water sample from wells in Vizcaino Biosphere Reserve, Mexico | 950 | 7.9 | [22] |
| **7** | Brackish and marine water in Aveiro, Portugal | 26,700<br>33,700 | 7.8<br>8.1 | [23] |
| **8** | Brackish water in Al-Asfar Lake, Saudi Arabia | 6,265 | 7.8 | [24] |
| **9** | Acı Lake, Denizli, Turkey | 31,500 | 8.4 | [25] |
| **10** | Groundwater in Dead Sea Basin | (~1,000 μS $cm^{-1}$) | 7.5-7.8 | [26] |
| **11** | Natural groundwater in Lilla tunnel, Spain | ~2,000 | 7.7 | [27] |
| **12** | Groundwater in Madurai district, India | 5,033 | 8.0 | [28] |
| **13** | Raw water in central Iran | 1,000-4,270 | 6.0-7.8 | [29] |
| **14** | Seawater in the coast of Sanya, China | ~35,000 | 8.15 | [30] |
| **15** | Seawater in the coast of Alexandria, Egypt | 36,544 | 7.6 | [31] |
| **16** | Seawater in Victoria habour, Hong Kong | 36,700 | 7.8 | [32] |
| **17** | Seawater in South China Sea | ~35,000 | 7.9-8.3 | [33] |
| **18** | Seawater | ~35,000 | 7.5-8.4 | [34] |
| **19** | Seawater, Paula | ~35,000 | 7.6-8.1 | [35] |
| **20** | Seawater, Chesapeake Bay, Danish Straits, Southern North Sea, Tampa Bay | ~35,000 | 7.9-8.4 | [36] |

[a] The pH of salt waters were measured at room temperature.

**Supplementary Table 2 |** The parameters of different adsorption models for the adsorption of $Na^+$ and $Cl^-$ by PSP-MIL-53.

| **Isotherm model**[a] | | **Calculated parameters** | | | |
|---|---|---|---|---|---|
| | | | $q_m$ (mg $g^{-1}$) | $b$ (L $mg^{-1}$) | $R^2$ |
| **Langmuir** | $\frac{1}{q_e}=\frac{1}{q_m}+\frac{1}{bq_mC_e}$ | UV | 86.21 | 0.00060 | 0.99 |
| | | Dark | 63.82 | 0.00055 | 0.96 |
| | | | $n$ | $K_f$ ($mg^{1-1/n}$ $L^{1/n}$ $g^{-1}$) | $R^2$ |
| **Freundlich** | $lnq_e=lnK_f+\frac{1}{n}lnC_e$ | UV | 3.00 | 3.10 | 0.88 |
| | | Dark | 2.98 | 2.24 | 0.76 |
| | | | $K_1$ | $K_2$ (L $mg^{-1}$) | $R^2$ |
| **Tempkin** | $q_e=K_1lnK_2+K_1lnC_e$ | UV | 15.52 | 0.0085 | 0.96 |
| | | Dark | 10.86 | 0.010 | 0.84 |

[a] $b$ is the Langmuir model constant, and $q_m$ is the maximum adsorption loading. $K_f$ and $n$ are the Freundlich constants. $K_1$ and $K_2$ are the Tempkin constants.

**Supplementary Table 3 |** The performance of common ion adsorbents/ion exchangers for desalination.

| Materials | NaCl concentration (ppm) | Ion adsorption | | Regeneration | | Ref. |
|---|---|---|---|---|---|---|
| | | Capacity (mmol $g^{-1}$)[a] | Time (min) | Method | Time (min) | |
| Amberlite IRA-68 and Amberlite IRC-84 (Desal process) | 500-3,000 | 1.8 (mmol $mL^{-1}$) | -- | $NH_4OH$ and $H_2SO_4$ solution | -- | [37] |
| Mixture of Amberlite IR-120 and Amberlite IR-410 | 100, 35,000 mixed salts | 1.0 (mmol $mL^{-1}$) | -- | 10% $H_2SO_4$ solution, NaOH solution | -- | [38] |
| Sirotherm desalination resin | 1,170 (pH 5.6) | 1.4-4.2 | 20-50 | Wash with 2M HCl and 0.3M NaOH, then heat at 80 °C | 20-30 | [39,40] |
| Sirotherm resin XPAA(EPEI.XG) | 5,850 (pH 4-5) | 1.6 | 20 | Heat treatment at 80-90 °C | -- | [41] |
| Mixed bed resin with $–COO^-$ and $–NR_2H^+$ | 5,850-29,250 (pH 5.6) | 1.0 | 900 | A combination of $NH_4HCO_3$ washing and heat treatment at 80 °C | 60 | [42] |
| Amberlite XD-2 | 3,700 (pH 5.5) | 2.0 | 20 | 90-95 °C water | -- | [43] |
| Sirotherm TR-20 | 2,000 (pH 5.6) | 2.8 | 120 | Heat treatment at 70 °C | 90 | [44] |
| PDMVBA-MIL-121 | 500-60,000 | 1.8 | 300 | Heat treatment at 80 °C | 960 | [7] |
| PSP-MIL-53 | 500-35,000 (pH 8) | 2.88 | 30 | Sunlight irradiation | 4 | This work |

[a] The unit of ion adsorption capacity is mmol $g^{-1}$ unless specified.

**Supplementary Table 4 |** The ionic radii, hydrated ionic radii and Gibbs free energies for hydration of ions.

| Ion | Ionic radius (Å) | Hydrated radius (Å)[45,46] | Gibbs free energy of hydration (kJ mol$^{-1}$)[46] |
|---|---|---|---|
| $Li^+$ | 0.69 | 3.82 | −475 |
| $Na^+$ | 0.95 | 3.58 | −365 |
| $K^+$ | 1.33 | 3.31 | −295 |
| $Mg^{2+}$ | 0.65 | 4.4 | −1,830 |
| $Ca^{2+}$ | 0.99 | 4.2 | −1,505 |
| $Cl^-$ | 1.81 | 3.32 | −340 |
| $HCO_3^-$ | 1.56 | 4.39[47-49] | −335 |
| $NO_3^-$ | 1.79 | 3.40 | −300 |
| $SO_4^{2-}$ | 2.30 | 3.79[50] | −1,080 |

**Supplementary Table 5 |** Scale up column design parameters and running parameters.

| Adsorbent in a column | | Single column parameters | |
|---|---|---|---|
| Amount (kg) | 451.70 | Diameter (m) | 0.97 |
| Product fresh water volume ($m^3$) | 10 | Adsorbent height (m) | 2 |
| Packing density (g $L^{-1}$) | 607 | Column height (m) | 3.5 |
| Volume ($m^3$) | 0.74 | Feed flow rate ($m^3$ $h^{-1}$) | 2.96 |
| Volume of adsorbent & glass beads ($m^3$) | 1.48 | Fresh water for regeneration ($m^3$) | 1.13 |
| | | Brine concentration (ppm) | 14,716 |

**Supplementary Table 6 |** Energy consumption of the two-bed desalination system.

| Pumps | | Lighting | | Energy consumption | |
|---|---|---|---|---|---|
| Motor power (kW) | 0.19 | Energy (kWh) | 43/1,000h | Pumps (kWh $m^{-3}$) | 0.096 |
| Flow rate ($m^3$ $h^{-1}$) | 3 | Intensity (lx) | 14,130 | Lighting (kWh $m^{-3}$) | 0.010 |
| Discharge head (m) | 7.3 | Spot diameter (m) | 0.35 | Total (kWh $m^{-3}$) | 0.11 |
| numbers | 3 | numbers | 8 | | |

**Supplementary Table 7 |** Specific energy consumption (SEC) of desalination techniques.

| Techniques [a] | Feed | SEC (kWh $m^{-3}$) | Product water quality (ppm) | Refs. |
|---|---|---|---|---|
| MSF | [b] | 19.6-27.3 | ~10 | 51,52 |
| MED | [b] | 14.5-21.4 | ~10 | 51,52 |
| SWRO | Seawater | 4-6 | 400-500 | 51,53 |
| BWRO | Brackish water | 1.5-2.5 | 200-500 | 51,53 |
| ED | Brackish water | 0.7-2.5 (<2,500 ppm)<br>2.6-5.5 (2,500-5,000 ppm) | 150-500 | 52,54,55 |
| MCDI | Brackish water | 0.1-1.5 (<2,500 ppm)<br>1.5-3.5 (2,500-5,000 ppm) | ~300 | 56 |
| MD | [c] | >100 (thermal)<br>~1.0 (electricity) | <10 | 57 |
| PSP-MIL-53 adsorbent based desalination | Brackish water | 0.11 (2233 ppm) [d]<br>0.21 (2233 ppm) [e] | <600 | This work |

[a] MSF – multi-stage flash; MED – multiple effect distillation; SWRO – seawater reverse osmosis; BWRO – brackish water reverse osmosis; ED – electrodialysis; MCDI – membrane assisted capacitive deionization.

[b] MSF and MED processes are practically applied for seawater desalination.

[c] MD process is suitable for desalting salt waters with wide ranges of salinity[58].

[d] The SEC is estimated with sunlight for regeneration during daytime (12 hours), and room lighting at night.

[e] The SEC is estimated with room lighting for the whole regeneration process.

## References


1 Loiseau, T. *et al.* A rationale for the large breathing of the porous aluminum terephthalate (MIL-53) upon hydration. *Chem. Eur. J.* **10**, 1373-1382 (2004).

2 Llewellyn, P. L. *et al.* Prediction of the conditions for breathing of metal organic framework materials using a combination of X-ray powder diffraction, microcalorimetry, and molecular simulation. *J. Am. Chem. Soc.* **130**, 12808-12814 (2008).

3 Boutin, A. *et al.* Breathing Transitions in MIL-53 (Al) Metal–Organic Framework Upon Xenon Adsorption. *Angew. Chem. Int. Ed.* **48**, 8314-8317 (2009).

4 Wang, C., Liu, X., Demir, N. K., Chen, J. P. & Li, K. Applications of water stable metal–organic frameworks. *Chem. Soc. Rev.* **45**, 5107-5134 (2016).

5 Zhao, X. *et al.* The stability and defluoridation performance of MOFs in fluoride solutions. *Microporous Mesoporous Mater.* **185**, 72-78 (2014).

6 Vu, T. A. *et al.* Arsenic removal from aqueous solutions by adsorption using novel MIL-53(Fe) as a highly efficient adsorbent. *RSC Adv.* **5**, 5261-5268 (2015).

7 Ou, R. *et al.* Thermoresponsive Amphoteric Metal–Organic Frameworks for Efficient and Reversible Adsorption of Multiple Salts from Water. *Adv. Mater.* **30**, 1802767 (2018).

8 Sahli, M. M. *et al.* Fluoride removal for underground brackish water by adsorption on the natural chitosan and by electrodialysis. *Desalination* **212**, 37-45 (2007).

9 Kim, D., Ahn, Y. H. & Lee, H. Phase Equilibria of CO2 and CH4 Hydrates in Intergranular Meso/Macro Pores of MIL-53 Metal Organic Framework. *J. Chem. Eng. Data* **60**, 2178-2185 (2015).

10 Nivetha, R. *et al.* Role of MIL-53(Fe)/hydrated-dehydrated MOF catalyst for electrochemical hydrogen evolution reaction (HER) in alkaline medium and photocatalysis. *RSC Adv.* **9**, 3215-3223 (2019).

11 Guillou, N., Millange, F. & Walton, R. I. Rapid and reversible formation of a crystalline hydrate of a metal-organic framework containing a tube of hydrogen-bonded water. *Chem. Commun.* **47**, 713-715 (2011).

12 Boyd, P. G. *et al.* Data-driven design of metal-organic frameworks for wet flue gas CO2 capture. *Nature* **576**, 253-256 (2019).

13 Gao, Q., Xu, J. & Bu, X. H. Recent advances about metal-organic frameworks in the removal of pollutants from wastewater. *Coordin. Chem. Rev.* **378**, 17-31 (2019).

14 Hai-Lang, Z. & Shi-Jun, H. Viscosity and density of water+ sodium chloride+ potassium chloride solutions at 298.15 K. *J. Chem. Eng. Data* **41**, 516-520 (1996).

15 Boix, G. *et al.* MOF-Beads Containing Inorganic Nanoparticles for the Simultaneous Removal of Multiple Heavy Metals from Water. *ACS Appl. Mater. Interfaces* **12**, 10554-10562 (2020).

16 Meng, X. C. & Zhang, Z. S. Experimental analysis of a photoreactor packed with Pd-BiVO4-Coated glass beads. *Aiche J.* **65**, 132-139 (2019).

17 Gunaratne, H. Q. N. *et al.* 'All in one' photo-reactor pod containing TiO2 coated glass beads and LEDs for continuous photocatalytic destruction of cyanotoxins in water. *Environ. Sci.: Water Res. Technol.* **6**, 945-950 (2020).

18 Topçuoğlu, S., Güngör, N. & Kirbaşoğlu, Ç. Physical and chemical parameters of brackish water lagoon, Küçükçekmece Lake, in northwestern Turkey. *Toxicol. Environ. Chem.* **69**, 101-108 (1999).
19 Ben Sik Ali, M., Hamrouni, B. & Dhahbi, M. Electrodialytic defluoridation of brackish water: effect of process parameters and water characteristics. *CLEAN–Soil Air Water* **38**, 623-629 (2010).
20 Lindholm, T., Öhman, P., Kurki-Helasmo, K., Kincaid, B. & Meriluoto, J. Toxic algae and fish mortality in a brackish-water lake in Åland, SW Finland. *Hydrobiologia* **397**, 109-120 (1999).
21 Hilles, A. H. & Al-Najar, H. Brackish water desalination is the merely potable water potential in the Gaza Strip: prospective and limitations. *J. Environ. Sci. Technol.* **4**, 158-171 (2011).
22 Brito-Castillo, L., Méndez Rodríguez, L., Chávez López, S. & Acosta Vargas, B. Groundwater differentiation of the aquifer in the Vizcaino Biosphere Reserve, Baja California Peninsula, Mexico. *Geofís. Int.* **49**, 167-179 (2010).
23 Santos, L. *et al.* Insights on the optical properties of estuarine DOM–hydrological and biological influences. *PloS one* **11**, e0154519 (2016).
24 Fathi, A., Al-Fredan, M. & Youssef, A. Water quality and phytoplankton communities in lake al-asfar, al-hassa, Saudi Arabia. *Res. J. Environ. Sci* **3**, 504-513 (2009).
25 Dalay, M. C. Arthrospira maxima (= Spirulina maxima (Stiz.) Geitl., 1930) Acı Lake Strain. *J. Fish Acquat. Sci* **19**, 241-245 (2002).
26 Al-Hadidi, M. M., Al Kharabsheh, A. A. & Ta'any, R. A. Impact of Over-Pumping on the Groundwater Quality of the Dead Sea Basin/Jordan. *Curr. World Environ.* **8**, 365-374 (2013).
27 Alonso, E., Berdugo, I. & Ramon, A. Extreme expansive phenomena in anhydritic-gypsiferous claystone: the case of Lilla tunnel. *Géotechnique* **63**, 584 (2013).
28 Thivya, C. *et al.* Identification of the geochemical processes in groundwater by factor analysis in hard rock aquifers of Madurai District, South India. *Arab. J. Geosci.* **7**, 3767-3777 (2014).
29 Davijani, M. H., Anvar, A. N. & Banihabib, M. Locating Water Desalination Facilities for Municipal Drinking Water Based on Qualitative and Quantitative Characteristics of Groundwater in Iran's Desert Regions. *Water Resour. Manag.* **28**, 3341-3353 (2014).
30 Wu, Z.-Z., Che, Z.-W., Wang, Y.-S., Dong, J.-D. & Wu, M.-L. Identification of surface water quality along the coast of Sanya, South China Sea. *PloS one* **10**, e0123515 (2015).
31 Kandeel, A. M., El-Mahllawy, M. S., Hassan, H. A., Sufe, W. H. & Zeedan, S. R. Effect of Sea Water and Sand Dunes on the Physico-Mechanical Properties of Magnesia Cement Masonry Units. *Trends Adv. Sci. Eng.* **1**, 2-13 (2011).
32 Li, X. & Zhao, Q. MAP precipitation from landfill leachate and seawater bittern waste. *Environ. Technol.* **23**, 989-1000 (2002).
33 Liu, Y. *et al.* Instability of seawater pH in the South China Sea during the mid-late Holocene: Evidence from boron isotopic composition of corals. *Geochim. Cosmochim. Acta* **73**, 1264-1272 (2009).
34 Chester, R. *Marine geochemistry*. 2nd Edition edn, (John Wiley & Sons, 2009).

35 Barkley, H. C. *et al.* Changes in coral reef communities across a natural gradient in seawater pH. *Sci. Adv.* **1**, e1500328 (2015).
36 Duarte, C. M. *et al.* Is ocean acidification an open-ocean syndrome? Understanding anthropogenic impacts on seawater pH. *Estuar. Coast.* **36**, 221-236 (2013).
37 Kunin, R. Further studies on the weak electrolyte ion exchange resin desalination process (Desal Process). *Desalination* **4**, 38-44 (1968).
38 Kunin, R. & McGarvey, F. X. Monobed deionization with ion exchange resins. *Ind. Eng. Chem.* **43**, 734-740 (1951).
39 Bolto, B., Eppinger, K., Jackson, M. & Siudak, R. An ion-exchange process with thermal regeneration XIV thermally regenerable resin systems with high capacities. *Desalination* **34**, 171-188 (1980).
40 Bolto, B. *et al.* An ion exchange process with thermal regeneration IX. A new type of rapidly reacting ion-exchange resin. *Desalination* **13**, 269-285 (1973).
41 Chanda, M., Pillay, S. A., Sarkar, A. & Modak, J. M. A thermally regenerable composite sorbent of crosslinked poly (acrylic acid) and ethoxylated polyethyleneimine for water desalination by sirotherm process. *J. Appl. Polym. Sci.* **111**, 2741-2750 (2009).
42 Chandrasekara, N. G. N. & Pashley, R. Study of a new process for the efficient regeneration of ion exchange resins. *Desalination* **357**, 131-139 (2015).
43 Hsu, T. B. & Pigford, R. L. Mass transfer in a thermally regenerable ion-exchange resin by continuous cycling. *Ind. Eng. Chem. Res.* **30**, 1067-1075 (1991).
44 Goto, S., Sato, N. & Teshima, H. Periodic Operation for Desalting Water with Thermally Regenerable Ion-Exchange Resin. *Sep. Sci. Technol.* **14**, 209-217 (1979).
45 Tansel, B. *et al.* Significance of hydrated radius and hydration shells on ionic permeability during nanofiltration in dead end and cross flow modes. *Sep. Purif. Technol.* **51**, 40-47 (2006).
46 Marcus, Y. Thermodynamics of solvation of ions. Part 5.—Gibbs free energy of hydration at 298.15 K. *J. Chem. Soc. Faraday Trans.* **87**, 2995-2999 (1991).
47 Geise, G. M., Cassady, H. J., Paul, D. R., Logan, B. E. & Hickner, M. A. Specific ion effects on membrane potential and the permselectivity of ion exchange membranes. *Phys. Chem. Chem. Phys.* **16**, 21673-21681 (2014).
48 Nightingale Jr, E. Phenomenological theory of ion solvation. Effective radii of hydrated ions. *J. Phys. Chem.* **63**, 1381-1387 (1959).
49 Kiriukhin, M. Y. & Collins, K. D. Dynamic hydration numbers for biologically important ions. *Biophys. Chem.* **99**, 155-168 (2002).
50 Paul, S., Choi, K. S., Lee, D. J., Sudhagar, P. & Kang, Y. S. Factors affecting the performance of supercapacitors assembled with polypyrrole/multi-walled carbon nanotube composite electrodes. *Electrochim. Acta* **78**, 649-655 (2012).
51 Semiat, R. Energy Issues in Desalination Processes. *Environ. Sci. Technol.* **42**, 8193-8201 (2008).
52 Al-Karaghouli, A. & Kazmerski, L. L. Energy consumption and water production cost of conventional and renewable-energy-powered desalination processes. *Renew. Sust. Energ. Rev.* **24**, 343-356 (2013).
53 Avlonitis, S. A., Kouroumbas, K. & Vlachakis, N. Energy consumption and membrane replacement cost for seawater RO desalination plants. *Desalination* **157**, 151-158 (2003).

54 Kuroda, O. *et al.* An electrodialysis sea water desalination system powered by photovoltaic cells. *Desalination* **67**, 33-41 (1987).
55 Adiga, M. R. *et al.* Performance analysis of photovolatic electrodialysis desalination plant at Tanote in Thar desert. *Desalination* **67**, 59-66 (1987).
56 Porada, S., Zhao, R., van der Wal, A., Presser, V. & Biesheuvel, P. M. Review on the science and technology of water desalination by capacitive deionization. *Prog. Mater. Sci.* **58**, 1388-1442 (2013).
57 Amy, G. *et al.* Membrane-based seawater desalination: Present and future prospects. *Desalination* **401**, 16-21 (2017).
58 Alsaadi, A. S., Francis, L., Maab, H., Amy, G. L. & Ghaffour, N. Evaluation of air gap membrane distillation process running under sub-atmospheric conditions: Experimental and simulation studies. *J. Membr. Sci.* **489**, 73-80 (2015).